Energy Materials

Supplementary Material

Designing the next generation of symmetrical organic redox flow batteries using helical carbocations

Jules Moutet, Tarek H. El-Assaad, Ramandeep Kaur, David D. Mills, Thomas L. Gianetti*

Department of Chemistry and Biochemistry, University of Arizona, Tucson, AZ 85719, USA.

Correspondence to: Prof. Thomas L. Gianetti, Department of Chemistry and Biochemistry, University of Arizona, 1306 E. University Blvd., Tucson, AZ 85719, USA. E-mail: tgianetti@arizona.edu

I. General Information

All solvents were purified by SPS or distillation over the drying agents indicated. Dried solvents and liquid reagents were transferred by oven-dried syringes or hypodermic syringes. The supporting electrolyte salts tetrabutylammonium hexafluorophosphate ($TBAPF_6$) and tetrabutylammonium tetrafluoroborate ($TBABF_4$) were recrystallized three times from ethanol, then dried at 80 ˚C for three days prior to use in glovebox. All glassware or hardware has been dried in an oven at least 24 h prior to introduction in glovebox.

NMR spectroscopy. ^{1}H, ^{13}C and ^{19}F NMR spectra were recorded on Bruker Avance III-400 MHz or DRX-500 MHz spectrometers in deuterated solvents using residual solvent signals as standards. The chemical shifts are expressed in δ (ppm). ^{1}H NMR signals multiplicities are designated as s (singlet), d (doublet), dd (doublet of doublet), dt (doublet of triplet), t (triplet), quin (quintet), m (multiplet), etc. Compounds naming has been done using ChemDraw (v19.0) and NMR spectra assignments were done using MestReNova (v14.1).

Electrochemistry. Electrochemical analyses were conducted inside an Argon-filled MBraun Unilab glovebox using a BioLogic SP-200 potentiostat/galvanostat and the EC-Lab® software (v11.50) from BioLogic Science Instruments. For convenience, potentials are expressed versus the internal reference electrode $AgNO_3$/Ag.

Facilities Acknowledgements

All NMR data were collected in the NMR facility of the Department of Chemistry and Biochemistry at the University of Arizona, RRID:SCR_012716. The purchase of the Bruker NEO 500 MHz spectrometer was supported by the National Science Foundation under Grant Number 1920234 and the University of Arizona.

II. Nomenclature

Supplementary Table 1: Molecules, acronyms, names, and references of the molecules presented in this work (all are *racemic*).

Molecule	Acronym	Common name	Reference
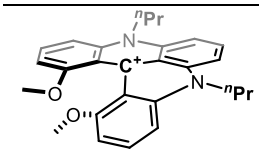	$^{n\mathrm{Pr}}$DMQA^{+}	N,N'-di-*n*-propyl-1,13-dimethoxy-quinacridinium	[1,2]
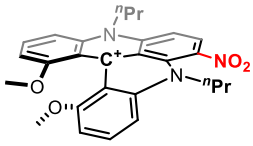	$^{n\mathrm{Pr}}$DMQA$^{\mathrm{NO2}+}$	N,N'-di-*n*-propyl-1,13-dimethoxy-6-nitro-quinacridinium	[3,4]
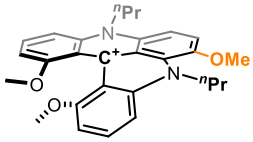	$^{n\mathrm{Pr}}$DMQA$^{\mathrm{OMe}+}$	N,N'-di-*n*-propyl-1,6,13-trimethoxy-quinacridinium	[3]
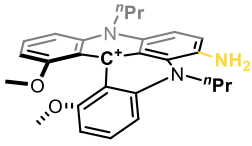	$^{n\mathrm{Pr}}$DMQA$^{\mathrm{NH2}+}$	N,N'-di-*n*-propyl-6-amino-1,13-dimethoxy-quinacridinium	[3]
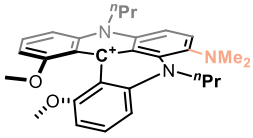	$^{n\mathrm{Pr}}$DMQA$^{\mathrm{NMe2}+}$	N,N'-di-*n*-propyl-6-(dimethylamino)-1,13-dimethoxy-quinacridinium	[3]
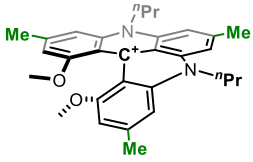	$^{n\mathrm{Pr}}$DMQA$^{(p\mathrm{Me})3+}$	N,N'-di-*n*-propyl-1,13-dimethoxy-3,7,11-trimethyl-quinacridinium	*This work*
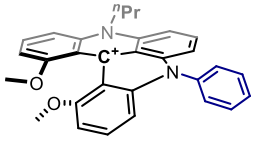	$^{n\mathrm{Pr/Ph}}$DMQA^{+}	N-*n*-propyl-N'-phenyl-1,13-dimethoxy-quinacridinium	[5]
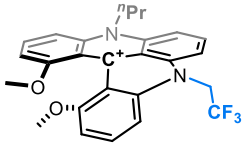	$^{n\mathrm{Pr/CH2CF3}}$DMQA^{+}	N-*n*-propyl-N'-(2,2,2-trifluoroethyl)-1,13-dimethoxy-quinacridinium	*This work*
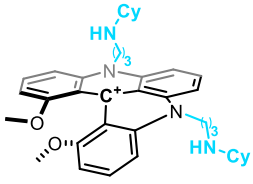	$^{(\mathrm{CyNHnPr})}$DMQA^{+}	N,N'-bis(3-(cyclohexylamino)propyl)-1,13-dimethoxy-quinacridinium	*This work*
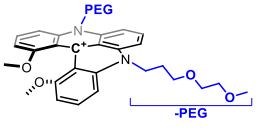	^{PEG}DMQA^{+}	N,N'-bis(3-(2-methoxyethoxy)propyl)-1,13-dimethoxy-quinacridinium	[6]
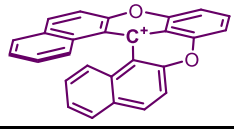	[6]helicene^{+}	benzo[a]benzo[5,6]chromeno[2,3,4-kl]xanthen-17c-ylium	[7]

III. Synthesis

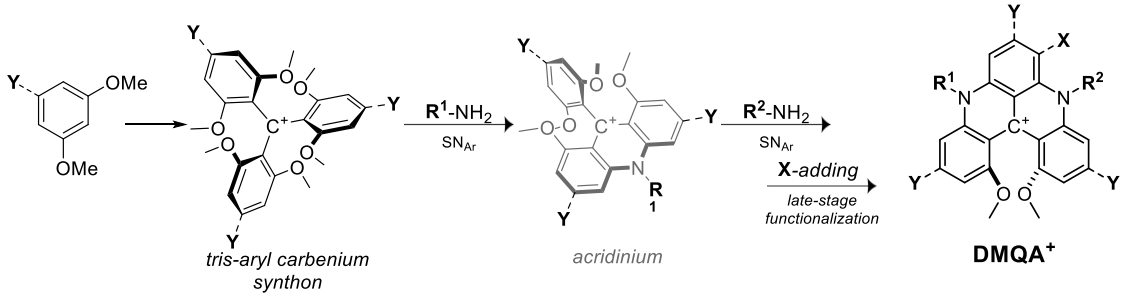

Supplementary Figure 1: General procedure for the synthesis of $^{R1/R2}DMQA^{X/Y+}$

The synthesis of compounds $^{nPr}DMQA^{+}$, $^{nPr}DMQA^{NO2+}$, $^{nPr}DMQA^{OMe+}$, $^{nPr}DMQA^{NH2+}$, $^{nPr}DMQA^{NMe2+}$, $^{nPr/Ph}DMQA^{+}$, PEGDMQA^{+} and [6]helicene^{+} are respectively detailed in the references indicated in the ***Supplementary Table 1****.*

<u>$^{nPr}DMQA^{(pMe)3+}$ synthesis route</u>

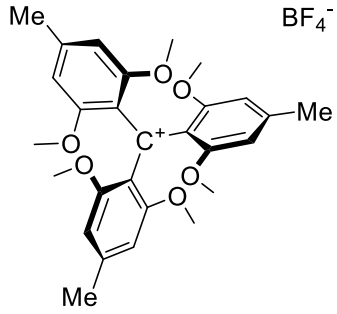

Tris(2,6-dimethoxy-4-methylphenyl)carbenium tetrafluoroborate

Into a degassed oven-dried 250 mL three-neck RBF equipped with a magnetic stirrer, a degassed solution of 3,5-dimethoxytoluene (4.85 g, 32 mmol, 1.0 equiv.) and freshly-distilled TMEDA (1.43 mL, 9.6 mmol, 0.3 equiv.) in 25 mL dry toluene was cannulated. The solution was cooled to 0 °C after which 1.6 M *n*-BuLi (22 mL, 35 mmol, 1.1 equiv.) was dropwise added while stirring under N_2 atmosphere. After the addition, the reaction was stirred for 1 h at room temperature, then a solution of diphenyl carbonate (2.03 g, 9.6 mmol, 0.3 equiv.) in 25 mL dry toluene was added via cannulation and the reaction was stirred for 15 h at 100 °C under N_2 atmosphere.

The reaction was cooled to rt, solvent was removed under reduced pressure and the yellowish orange residue was redissolved in CH_2Cl_2 (*ca.* 50 mL), washed with H_2O (50 mL), saturated $NaHCO_3$ (50 mL), then H_2O (50 mL). Solvent was removed under reduced pressure. The residue was dissolved in a minimum amount of methanol (*ca.* 10

mL) and $HBF_4.H_2O$ (8 mL, 48 wt%) was added dropwise. The mixture was stirred for 1 h at rt, after which Et_2O (250 mL) was added and stirring was continued for an additional 1 h. The crude was then obtained via vacuum filtration, washed with Et_2O (5 x 50 mL) then hexanes (3 x 50 mL).

The obtained solid was dissolved in MeCN and purified by precipitation from Et_2O to afford the title compound (3.00 g, 57%) as dark purple solid.

^{1}H NMR (500 MHz, $CDCl_3$): δ (ppm) = 6.32 (s, 6H), 3.56 (s, 18H), 2.42 (s, 9H).

^{13}C{^{1}H} NMR (126 MHz, $CDCl_3$): δ (ppm) = 176.0, 162.3, 154.6, 123.0, 105.8, 56.6, 23.6.

^{19}F{^{1}H} NMR (471 MHz, $CDCl_3$): δ (ppm) = -153.99, -154.0.

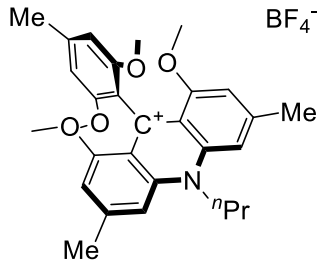

9-(2,6-dimethoxy-4-methylphenyl)-1,8-dimethoxy-3,6-dimethyl-10-propyl-9,10-dihydroacridin-9-ylium tetrafluoroborate

To a solution of tris(2,6-dimethoxy-4-methylphenyl)carbenium tetrafluoroborate (2.00 g, 3.62 mmol, 1.0 equiv.) in MeCN (10 mL) in a 50 mL RBF, *n*-propylamine (1.07 g, 18.1 mmol, 5.0 equiv.) was added. During the addition, a color change from purple to red was observed. The mixture was stirred for 90 min at rt, after which it was poured in Et_2O (250 mL) and stirred for an additional 30 min at rt. A precipitate was collected by vacuum filtration and washed with Et_2O (5 x 50 mL) then hexanes (3 x 50 mL). The obtained solid was dissolved in MeCN and purified by precipitation from Et_2O to afford the title compound (1.50 g, 76%) as orange reddish solid.

^{1}H NMR (500 MHz, $CDCl_3$): δ (ppm) = 7.55 (s, 2H), 6.76 (s, 2H), 6.46 (s, 2H), 5.04 – 4.98 (m, 2H), 3.54 (s, 12H), 2.71 (s, 6H), 2.47 (s, 3H), 2.26 – 2.17 (m, 2H), 1.34 (t, J = 7.4 Hz, 3H).

^{13}C{^{1}H} NMR (126 MHz, $CDCl_3$): δ (ppm) = 160.4, 156.0, 155.3, 152.6, 141.4, 139.4, 118.1, 116.5, 108.2, 108.1, 104.2, 56.7, 55.8, 52.8, 23.8, 22.2, 21.2, 10.9.

^{19}F{^{1}H} NMR (471 MHz, $CDCl_3$): δ (ppm) = -153.13, -153.18.

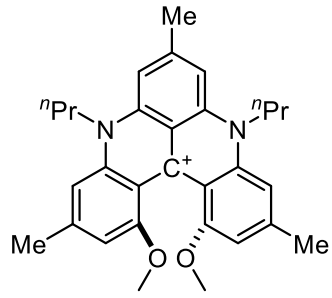

$^{n\mathrm{Pr}}$DMQA$^{(p\mathrm{Me})3+}$

N,N'-di-*n*-propyl-1,13-dimethoxy-3,7,11-trimethyl-quinacridinium described as $^{n\mathrm{Pr}}$DMQA$^{(p\mathrm{Me})3+}$

In a 15 mL cylindrical pressure vessel tube equipped with a magnetic stirrer, 9-(2,6-dimethoxy-4-methylphenyl)-1,8-dimethoxy-3,6-dimethyl-10-propyl-9,10-dihydroacridin-9-ylium tetrafluoroborate (500 mg, 0.91 mmol, 1.0 equiv.) was dissolved in MeCN (5 mL). After which *n*-propylamine (1.35 g, 22.8 mmol, 25 equiv.) was added. The mixture was stirred at 85 °C for 15 h. The dark blue mixture was then poured in Et_2O (150 mL) and stirred for 30 min at rt. A precipitate was collected by vacuum filtration and washed with Et_2O (5 x 25 mL) and hexanes (5x 25 mL). The obtained solid was purified by column chromatography (SiO_2, 1:9:0.2 MeCN/CH_2Cl_2/*i*PrOH) and the reddish green fractions were concentrated and then recrystallized from MeCN/Et_2O to afford the title compound (125 mg, 25%) as a dark bluish green solid.

^{1}H NMR (400 MHz, DMSO-d_6): δ (ppm) = 7.46 (s, 2H), 7.36 (s, 2H), 6.85 (s, 2H), 4.70 – 4.58 (m, 2H), 4.47 – 4.36 (m, 2H), 3.70 (s, 6H), 2.75 (s, 3H), 2.60 (s, 6H), 2.01 – 1.83 (m, 4H), 1.16 (t, J = 7.3 Hz, 6H).

^{13}C{^{1}H} NMR (126 MHz, DMSO-d_6): 159.5, 148.9, 148.6, 142.1, 141.4, 138.6, 117.1, 110.7, 107.6, 106.2, 105.1, 56.0, 23.8, 23.3, 19.7, 11.3.

^{19}F{^{1}H} NMR (471 MHz, DMSO-d_6): δ (ppm) = -148.24, -148.29.

^{n}Pr/CH2CF3DMQA^{+} synthesis route

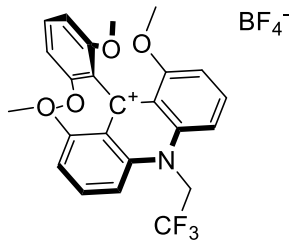

9-(2,6-dimethoxyphenyl)-1,8-dimethoxy-10-(2,2,2-trifluoroethyl)-9,10-dihydroacridin-9-ylium tetrafluoroborate

To a solution of tris(2,6 dimethoxyphenyl)carbenium tetrafluoroborate salt[8] (2.00 g, 3.98 mmol, 1.0 equiv) in acetonitrile (5 mL) in a pressure flask was added 2,2,2-Trifluoroethylamine (3.1 mL, 39.2 mmol, 10 equiv). The reaction mixture was heated at 80 °C for 18 h, then acetonitrile and the amine were removed under reduced pressure. The crude product was crashed using DCM/Et_2O, yielding a bright red solid (1.9 g, 88%).

^{1}H NMR (500 MHz, DMSO-d_6): δ (ppm) = 8.36 (t, J = 8.6 Hz, 1H), 8.28 (d, J = 9.3 Hz, 1H), 7.45 (t, J = 8.5 Hz, 0H), 7.28 (d, J = 7.9 Hz, 1H), 6.82 (d, J = 8.5 Hz, 1H), 6.50 (q, J = 8.6 Hz, 1H), 3.54 (s, 6H).

^{13}C{^{1}H} NMR (126 MHz, CD_3CN): 160.9, 160.1, 155.6, 142.7, 141.6, 130.1, 124.6 (q, J = 282.7 Hz), 119.6, 119.3, 110.3, 107.9, 104.3, 57.8, 56.4, 50.2 (q, J = 33.1 Hz).

^{19}F NMR (470 MHz, DMSO-d_6): δ (ppm) = -64.72, -148.24, -148.30.

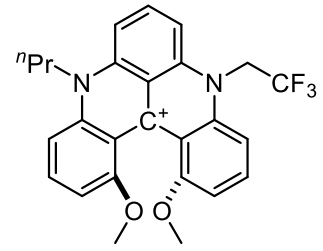

^{n}Pr/CH2CF3DMQA^{+}

N-*n*-propyl-N'-(2,2,2-trifluoroethyl)-1,13-dimethoxy-quinacridinium described as ^{n}Pr/CH2CF3DMQA^{+}

To a solution of 9-(2,6-dimethoxyphenyl)-1,8-dimethoxy-10-(2,2,2-trifluoroethyl)-9,10-dihydroacridin-9-ylium tetrafluoroborate (50 mg, 0.09 mmol, 1.0 equiv) in acetonitrile (5 mL) in a pressure flask was added n-propylamine (0.15 mL, 1.8 mmol, 20 equiv). The reaction mixture was heated at 100°C for 24h, then acetonitrile and n-propylamine were removed under reduced pressure. The crude product was crashed using DCM/Et_2O, yielding a green solid (20 mg, 40%).

^{1}H NMR (500 MHz, DMSO-*d*$_6$): δ (ppm) = 8.30 (t, *J* = 8.4 Hz, 1H), 8.02 (t, *J* = 8.3 Hz, 1H), 7.95 (t, *J* = 8.5 Hz, 2H), 7.84 (d, *J* = 8.5 Hz, 1H), 7.70 (d, *J* = 9.0 Hz, 2H), 7.05 (t, *J* = 8.6 Hz, 2H), 6.02 – 5.92 (m, 1H), 5.88 – 5.80 (m, 1H), 4.83 – 4.75 (m, 1H), 4.63 – 4.55 (m, 1H), 3.73 (s, 3H), 3.70 (s, 3H), 2.15 – 1.93 (m, 2H), 1.16 (t, *J* = 7.7 Hz, 3H).

^{13}C{^{1}H} NMR (126 MHz, DMSO-*d*$_6$): 159.1, 143.0, 141.8, 137.9, 137.1, 136.7, 129.6, 108.0, 103.7, 103.3, 55.8, 55.7, 30.6, 29.0, 20.8, 19.6, 10.7.

^{19}F{^{1}H} NMR (471 MHz, DMSO-*d*$_6$): -67.67, -151.71, -151.76.

$^{(CyNHnPr)}$DMQA^{+} synthesis route

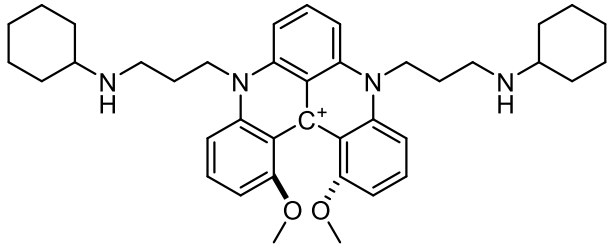

$^{(CyNHnPr)}$DMQA^{+}

To a purple solution of tris(2,6-dimethoxyphenyl)carbenium tetrafluoroborate salt[8] (300 mg, 0.59 mmol, 1 eq.) in acetonitrile (7mL), 2.5 equivalents of N-cyclohexylpropane-1,3-diamine (0.25 mL, 1.47 mmol, 2.5 eq.) were added under vigorous stirring. The reactional mixture quickly turned light red color. The reactional mixture was then warmed at 85 °C for 16 h during which it slowly turned deep greenish color. After total evaporation of acetonitrile, the blue-green residue was dissolved in the minimum amount of CH_3CN and precipitated 3 times by pouring and stirreded cold Et_2O. Suitable XRD crystals were obtained by slow vapor diffusion of diethyl ether by layering in a concentrated solution of the isolated precipitate in acetonitrile (343 mg, 83%).

^{1}H NMR (500 MHz, CD_3CN): δ (ppm) = 8.16 (t, J = 8.6 Hz, 1H), 7.89 (dd, J = 8.9, 8.0 Hz, 2H), 7.72 (d, J = 8.6 Hz, 2H), 7.64 (d, J = 8.9 Hz, 2H), 6.92 (d, J = 8.0 Hz, 2H), 4.80 (ddd, J = 15.7, 10.2, 5.9 Hz, 2H), 4.64 – 4.55 (m, 2H), 3.73 (s, 6H), 2.85 (t, J = 6.2 Hz, 4H), 2.44 (t, J = 10.7 Hz, 2H), 2.18 – 2.04 (m, 8H), 1.76 – 1.70 (m, 4H), 1.61 (dt, J = 12.6, 3.6 Hz, 2H), 1.34 – 1.04 (m, 12H).

^{13}C{^{1}H} NMR (126 MHz, CD_3CN): δ (ppm) = 160.5, 143.3, 143.1, 140.0, 137.7, 137.2, 120.3, 113.9, 108.7, 106.0, 103.8, 57.6, 56.4, 48.9, 44.2, 34.3, 28.0, 27.0, 25.7.

^{19}F{^{1}H} NMR (471 MHz, CD_3CN): δ (ppm) = -151.79, -151.84.

IV. Cyclic voltammograms

Cyclic voltammograms, determination of diffusion (D) and electron transfer rate (k0) parameters for compounds $^{nPr}DMQA^{+}$, $^{nPr}DMQA^{NO2+}$ *and* $^{PEG}DMQA^{+}$ *are available from their respective references cited in* **Supplementary Table *1***.

Cyclic voltammograms (CV) were measured in a three-electrode electrochemical cell, consisting of a platinum wire counter electrode (E_c), a $AgNO_3$/Ag reference electrode (E_{ref}, 0.01 M $AgNO_3$ in 0.1 M $TBAPF_6$ in CH_3CN), and a glassy carbon working electrode (E_w, 0.071 cm², CH Instrument, Inc.). The working electrode was polished prior each record using aluminium oxide on polishing paper and anhydrous CH_3CN to remove any residual particles.

Diffusion (*D*) and electron transfer rate (k^0) determination

Cyclic voltammograms were recorded at different scan rates (10, 25, 75, 100, 250, 400, and 500 mV/s) in an CH_3CN electrolyte containing 1 mM of desired $DMQA^+$ and 0.1M $TBAPF_6$ at 298K. For each compound not yet published, the peak current (I) *vs* square root of scan rate (ν) and linear fits for electronic processes at $E_{1/2}^{Red}$ (blue) and $E_{1/2}^{Ox}$ (green) have been plotted.

$$i_p = 0.4463nFAC\sqrt{\frac{nF\nu D}{RT}} \qquad (1)$$

Supplementary Equation 1. Randles-Sevcik equation, with i_p the peak current in Amperes, n equals the number of electrons transferred, F equals Faraday's constant, A is the area of the electrode in cm², C the concentration of redox active species in mol cm^{-3}, D the diffusion coefficient in cm^2 s^{-1}, v the scan rate in V s^{-1}, R the ideal gas constant, and T the temperature in Kelvin.

$$\psi = \frac{(-0.6288+0.0021\Delta E_p)}{(1-0.017\Delta E_p)} \qquad (2)$$

$$\psi = \frac{k^0}{\sqrt{\frac{\pi D n F v}{RT}}} \qquad (3)$$

Where: $\Delta E_p = (E_p^{max} - E_p^{min})$

Supplementary Equation 2-3. Nicholson's method[9] and the more recent work of reported by Lavagnini et al.[10] were used to determine the electron transfer rate constant (k^0) by relating it with the dimensionless kinetic parameter (Ψ). With *n* the number of electrons transferred, *F* equals Faraday's constant, *v* the scan rate, *R* the ideal gas constant and *T* the temperature in Kelvin. *D* diffusion coefficient at the corresponding scan rate.

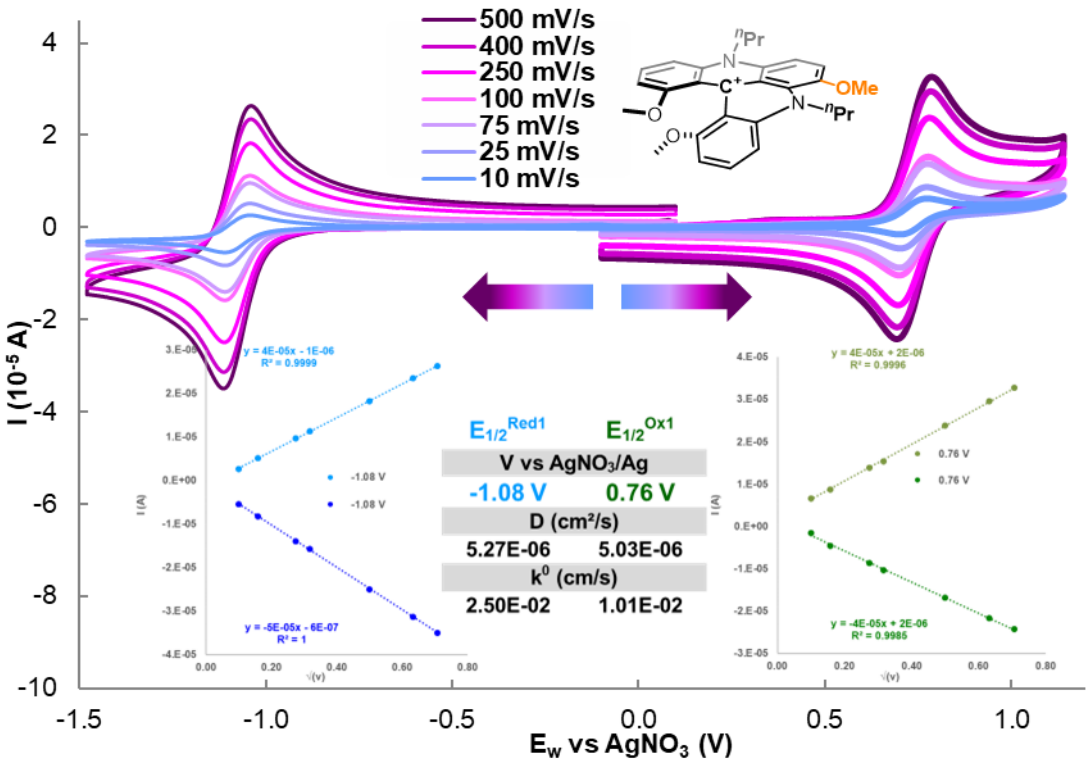

Supplementary Figure 2. Various scan rates CVs of $^{n\mathrm{Pr}}$DMQA$^{\mathrm{OMe}+}$. Plots display peak current (I) vs square root of scan rate (ν) alongside linear fits. Table summarizes $E_{1/2}$, D, and k^0.

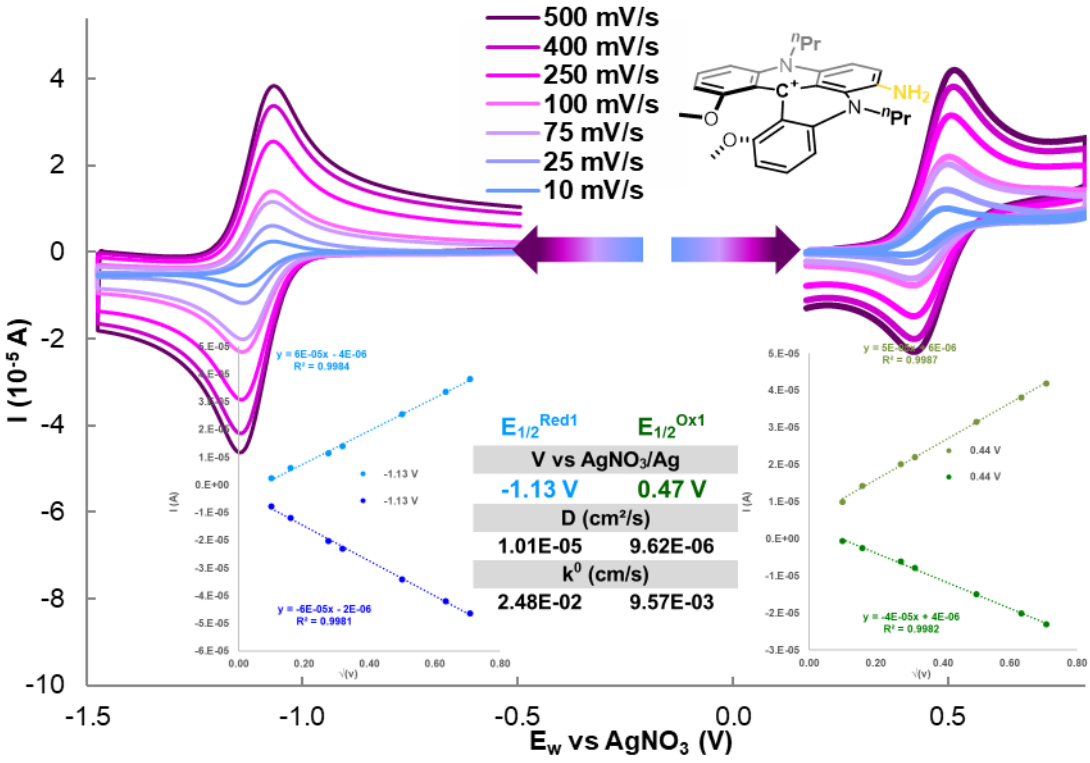

Supplementary Figure 3. Various scan rates CVs of $^{n\mathrm{Pr}}$DMQA$^{\mathrm{NH2}+}$. Plots display peak current (I) vs square root of scan rate (ν) alongside linear fits. Table summarizes $E_{1/2}$, D, and k^0.

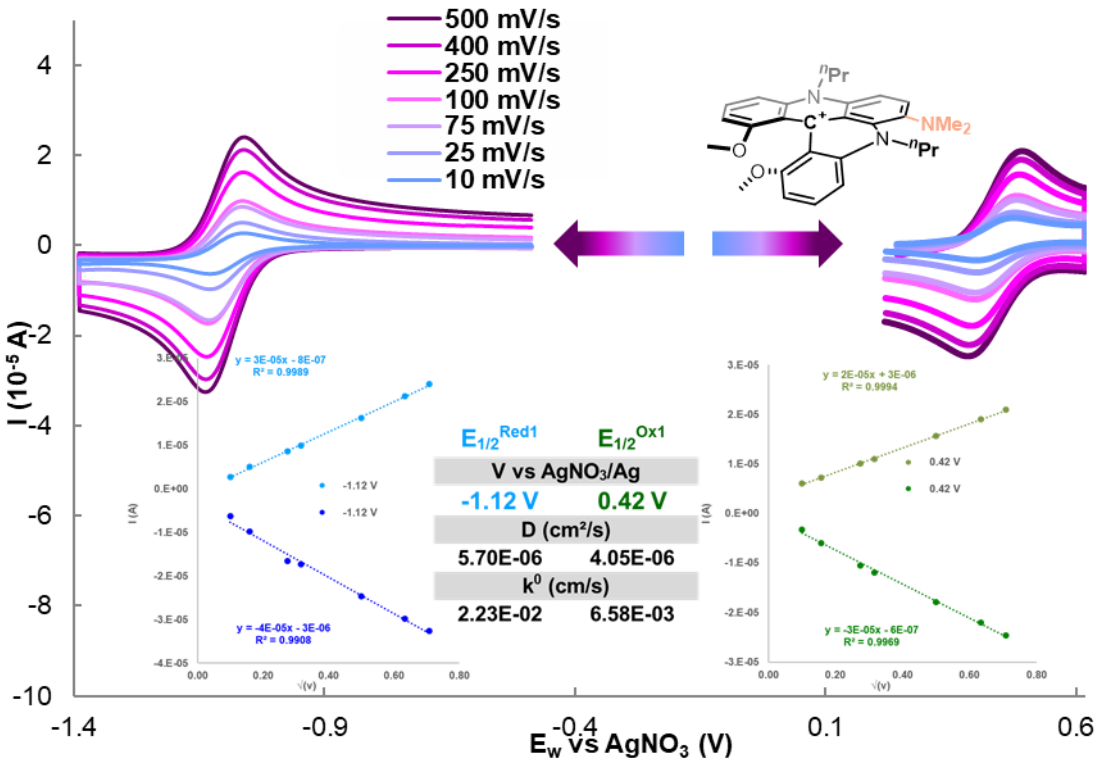

Supplementary Figure 4. Various scan rates CVs of $^{n\mathrm{Pr}}$DMQA$^{\mathrm{NMe2+}}$. Plots display peak current (I) vs square root of scan rate (ν) alongside linear fits. Table summarizes $E_{1/2}$, D, and k^0.

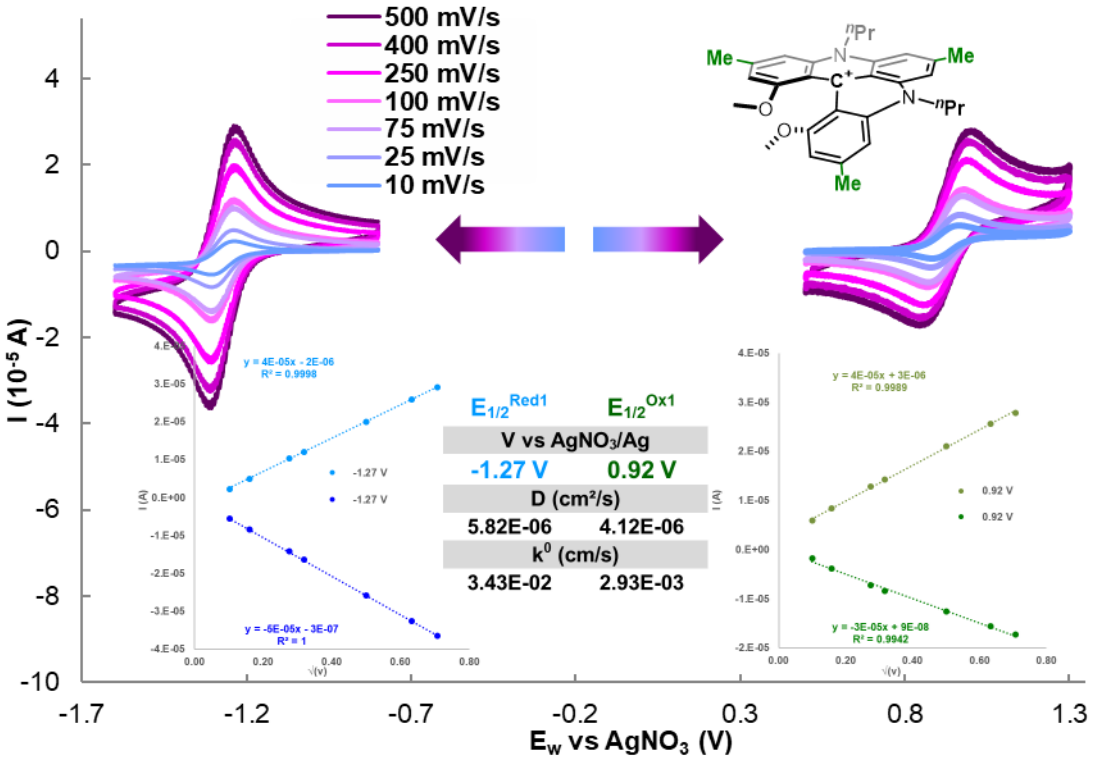

Supplementary Figure 5. Various scan rates CVs of $^{n\mathrm{Pr}}$DMQA$^{(p\mathrm{Me})3+}$. Plots display peak current (I) vs square root of scan rate (ν) alongside linear fits. Table summarizes $E_{1/2}$, D, and k^0.

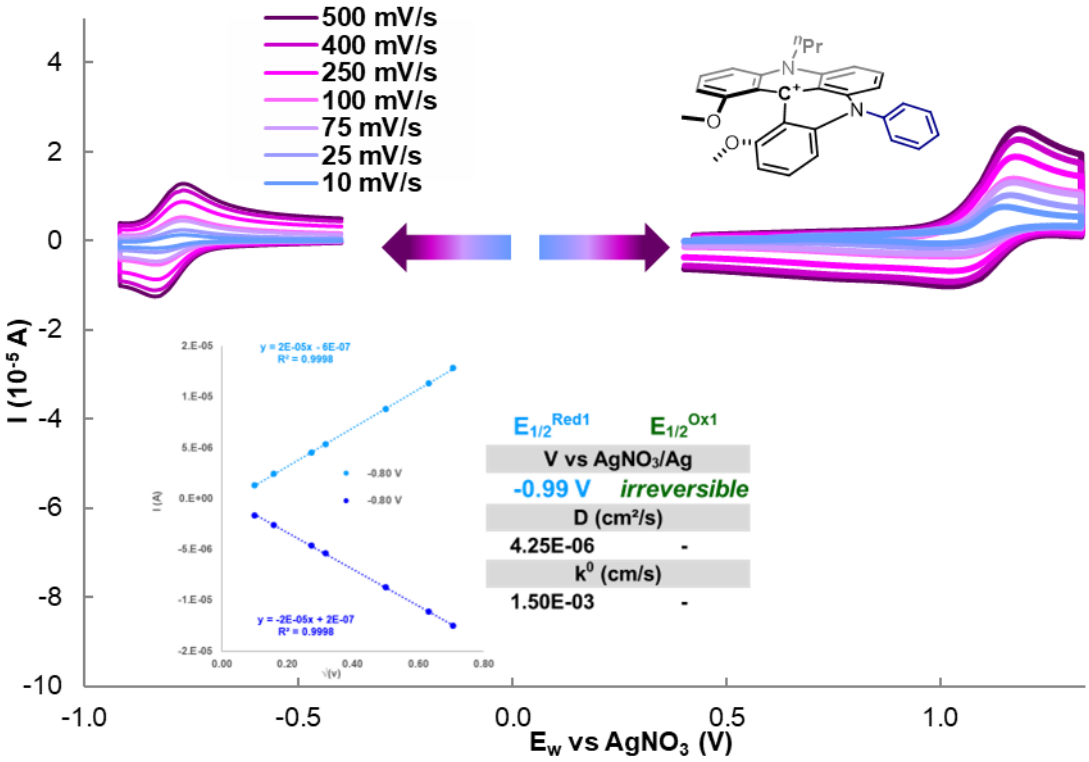

Supplementary Figure 6. Various scan rates CVs of $^{nPr/Ph}DMQA^{+}$. Plots display peak current (I) vs square root of scan rate (ν) alongside linear fits. Table summarizes $E_{1/2}$, D, and k^0.

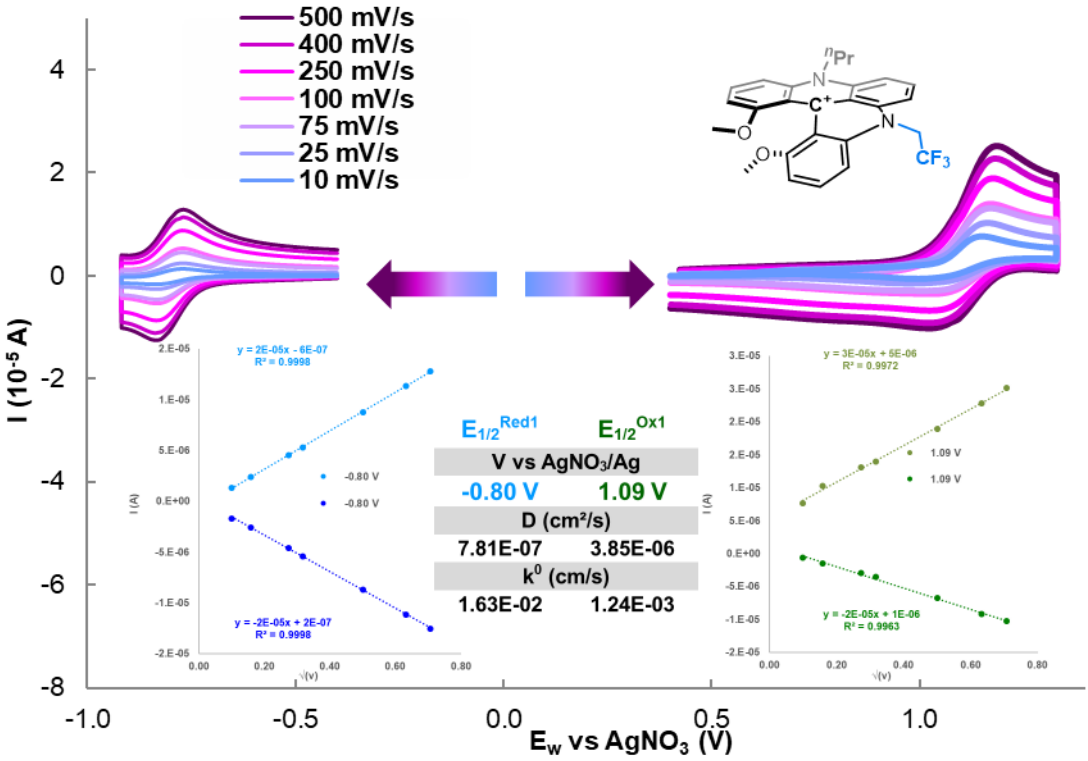

Supplementary Figure 7. Various scan rates CVs of $^{nPr/CH2CF3}DMQA^{+}$. Plots display peak current (I) vs square root of scan rate (ν) alongside linear fits. Table summarizes $E_{1/2}$, D, and k^0.

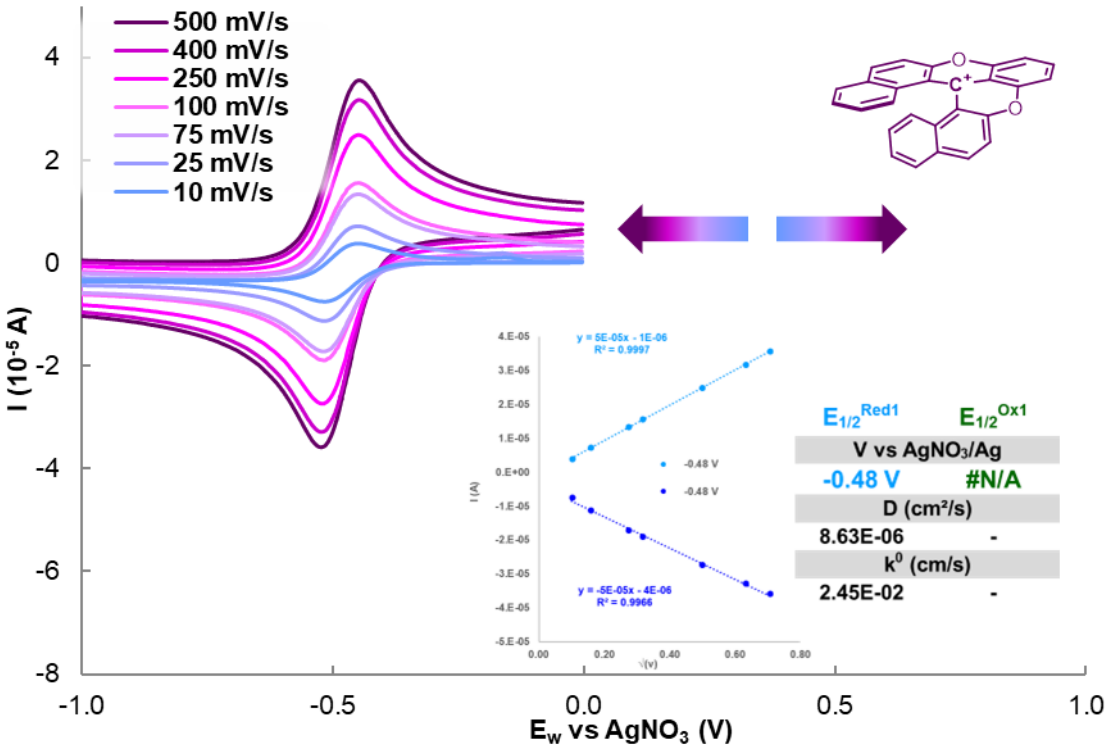

Supplementary Figure 8. Various scan rates CVs of [6]helicenium^{+}. Plots display peak current (I) vs square root of scan rate (ν) alongside linear fits. Table summarizes $E_{1/2}$, D, and k^0.

V. "Static RFB" – H-cell cycling

For 1 mM $^{R1/R2}DMQA^{X/Y+}$ dissolved in 0.1 M $TBABF_6$ in acetonitrile, an $AgNO_3/Ag$ quasi-reference electrode (0.01 M $AgNO_3$ in 0.1 M $TBAPF_6$ in CH_3CN) was used on the working side of the H-cell (E_w). Charging and discharging were all conducted with a current of |5| mA and the upper and lower voltage cutoffs were ±0.3 V the $E_{1/2}^{Red}$ (determined with CV at various scan rate from 10 mV/s to 500 mV/s and DPV) with reduction process $DMQA^+/DMQA^\bullet$ at the E_w.

Bulk charge/discharge measurements were carried out in a custom H-cell (pictured below) with a 2 mm fine porous glass frit (4-5.5µm pores diameter) was used as separator.[11,12] The working and counter electrodes were Reticulated vitreous carbon (RVC) electrodes (100 ppi Duocel® 3% relative density) were cut into rods of dimensions 0.5 cm × 0.5 cm × 4 cm and positioned about 2 cm deep in solution (active surface ~ 33 cm² per electrode). To rule out contamination processes, the electrodes were singly used. A Constant Current followed by a Constant Voltage Galvanostatic Charging with Potential Limitation (CCCV GCPL protocol) was applied *via* RVC electrodes. Both chambers of the H-cell were loaded with 5 mL of electrolyte/ROM and were continuously stirred with magnetic stir bars at 1000 rpm. An equilibration period of 2 h was used before active charging and discharging. Each battery has been cycled at least until their capacity drops below 50%. Results of H-cell bulk electrolysis are displayed below in graphs of normalized discharge capacity (normalized relative to theoretical capacity) and coulombic efficiency vs number of charge-discharge cycles. Based mainly on diffusion effects, the H-cell experiments do not provide relevant energy efficiency (EE) values, as the solutions are greatly affected by the Joule effect imposed on the solutions, so the EE is not displayed.

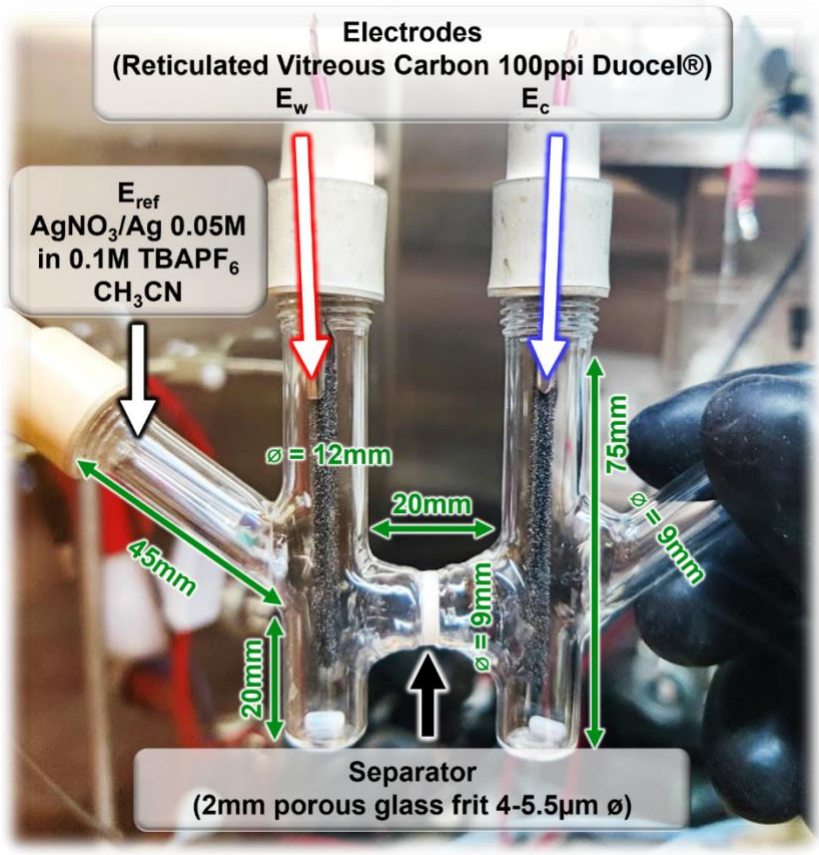

Supplementary Figure 9. Homemade H-cell picture with dimensions, diameters, and electrodes setup.

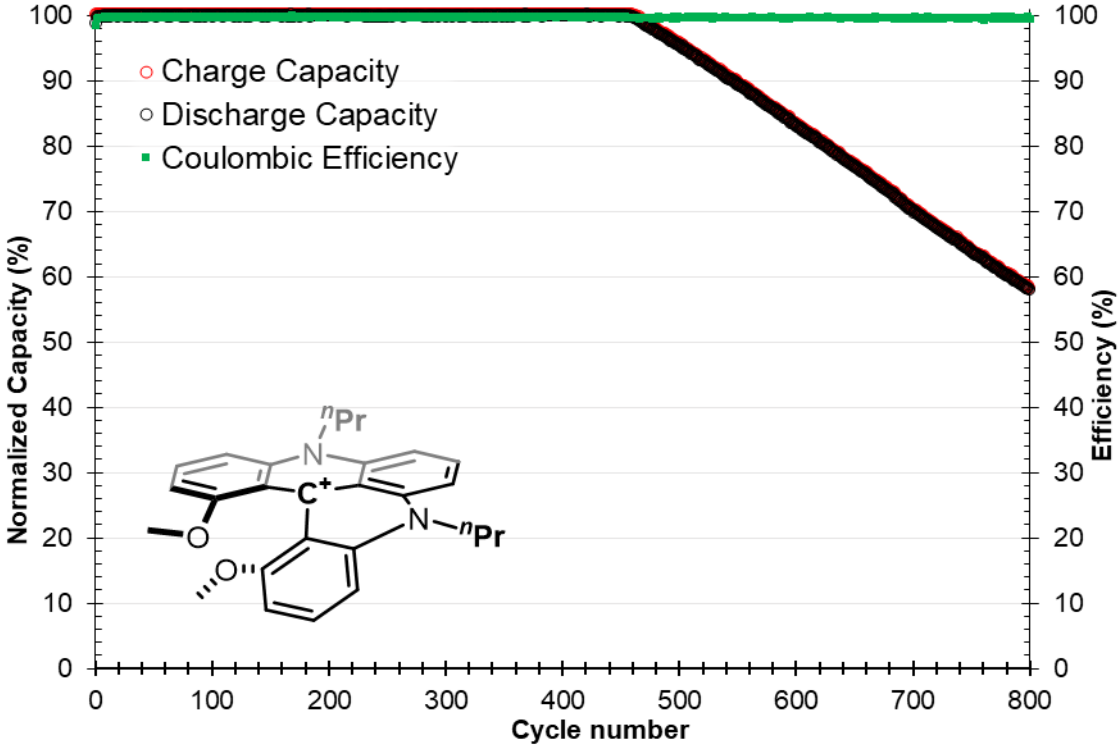

Supplementary Figure 10. $^{n\mathrm{Pr}}$DMQA^{+}.Coulombic Efficiency and Capacity monitoring. Each data point represents one cycle.

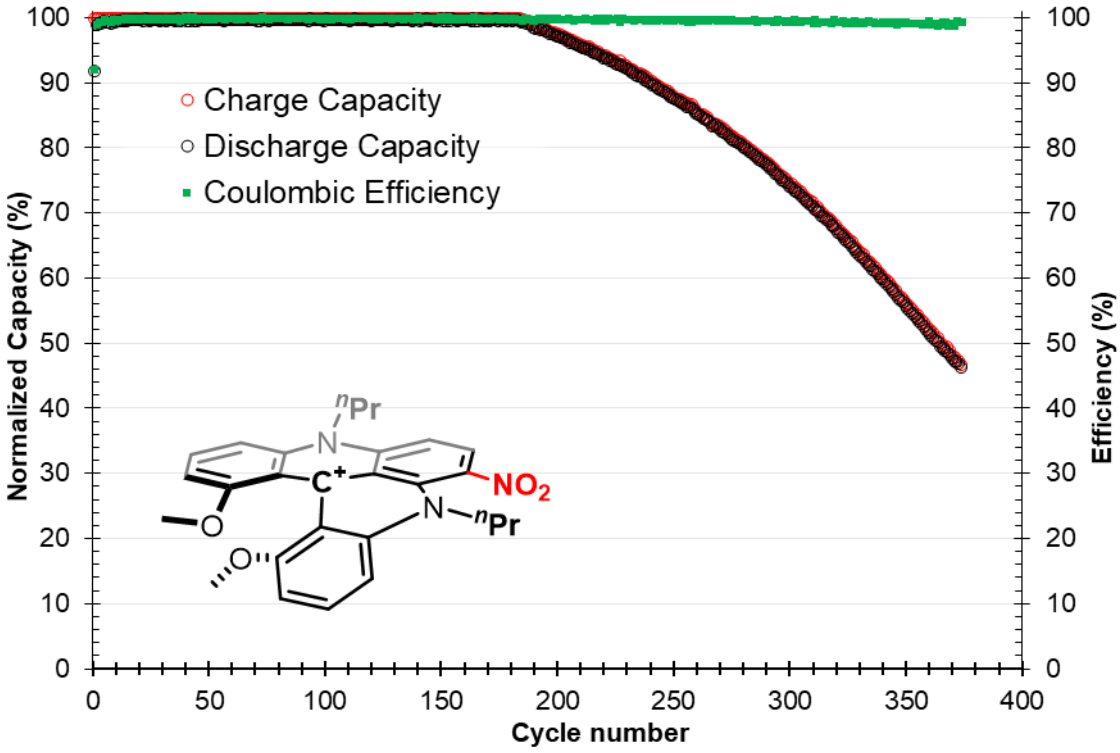

Supplementary Figure 11. $^{n\mathrm{Pr}}$DMQA$^{\mathrm{NO2+}}$.Coulombic Efficiency and Capacity monitoring. Each data point represents one cycle.

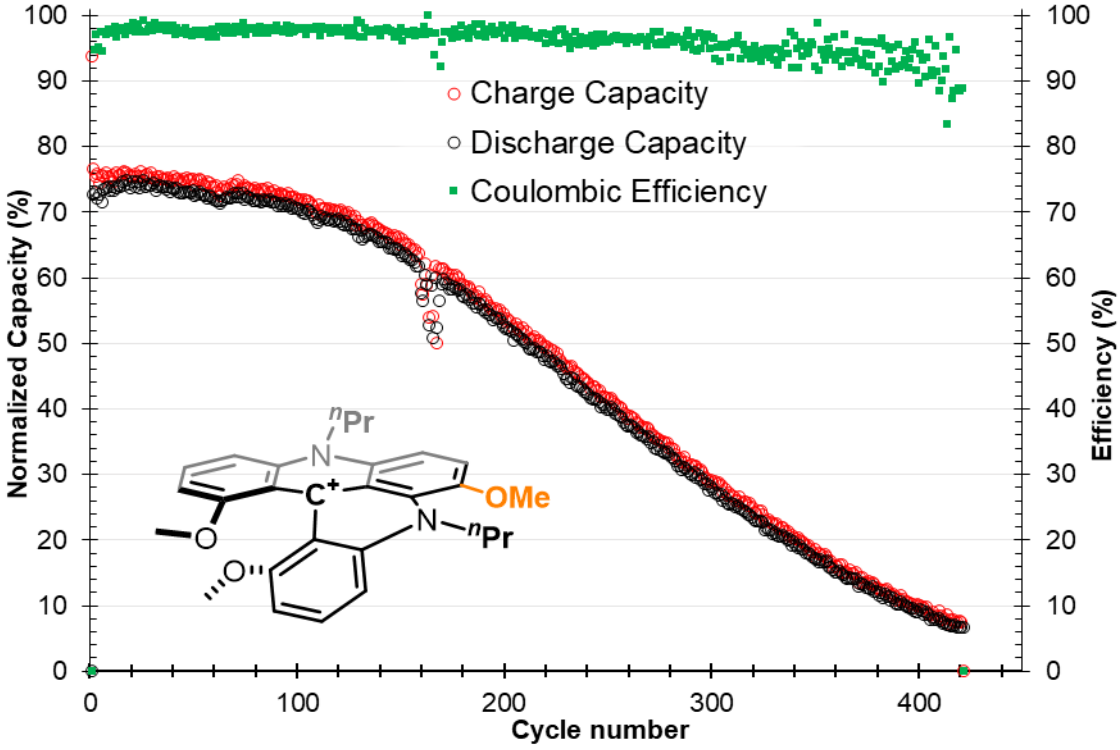

Supplementary Figure 12. $^{n\mathrm{Pr}}$DMQA$^{\mathrm{OMe+}}$.Coulombic Efficiency and Capacity monitoring. Each data point represents one cycle.

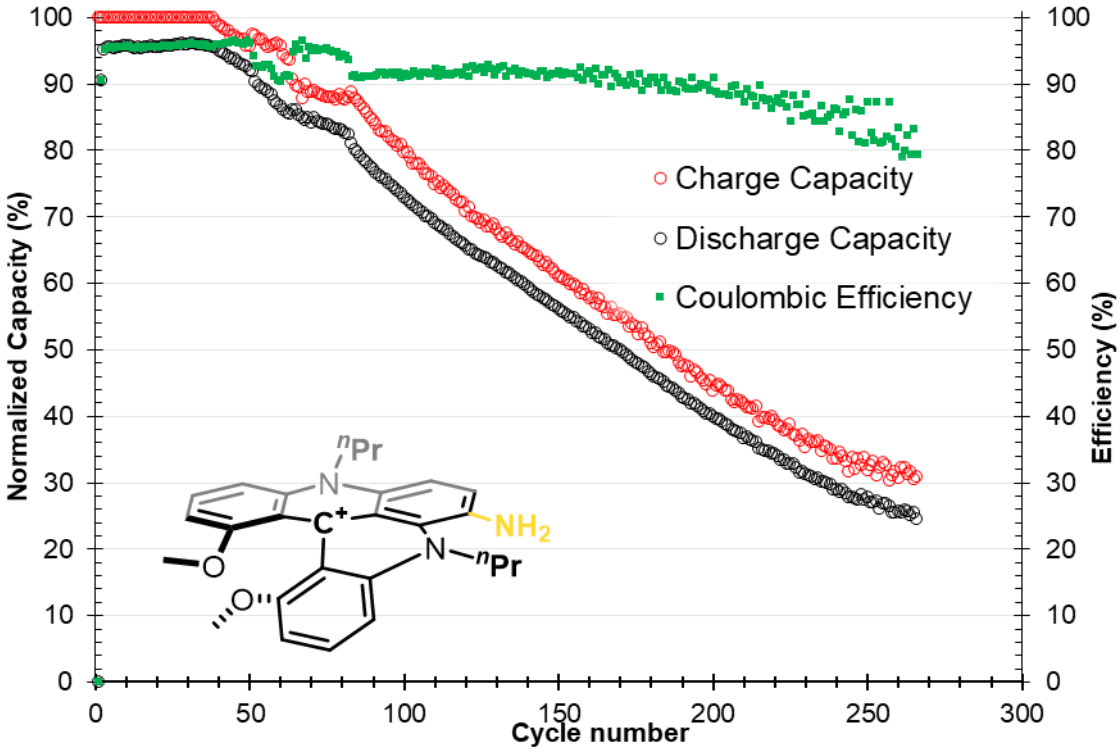

Supplementary Figure 13. $^{n\mathrm{Pr}}$DMQA$^{\mathrm{NH2+}}$.Coulombic Efficiency and Capacity monitoring. Each data point represents one cycle.

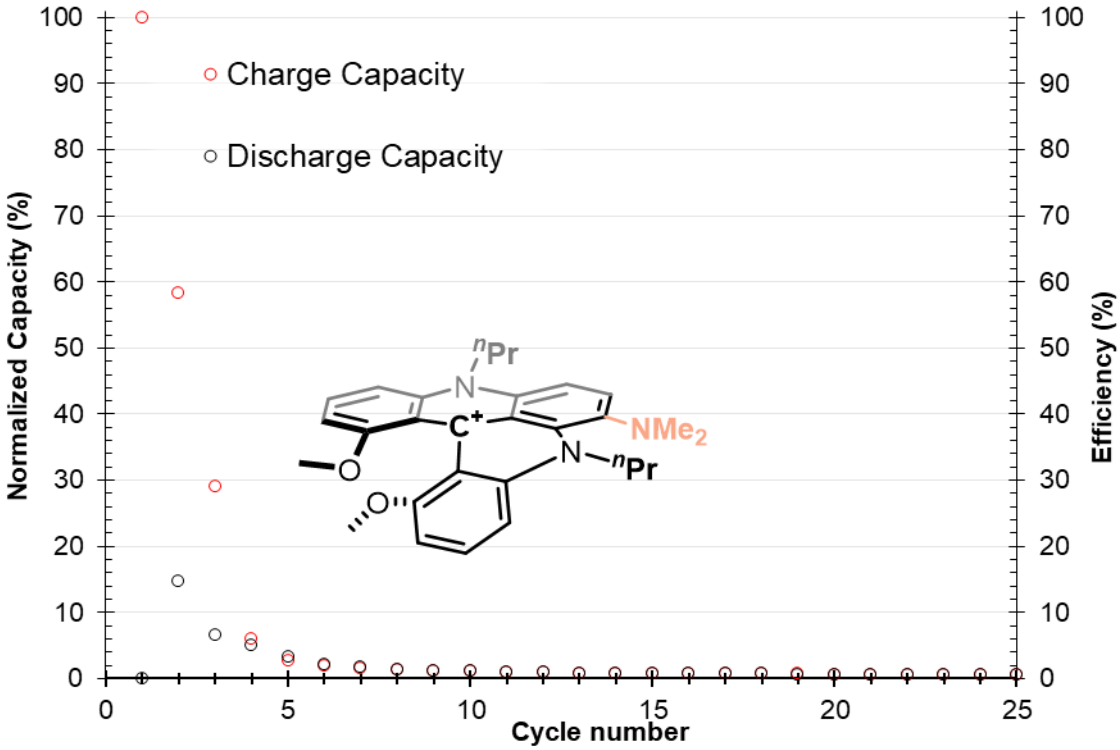

Supplementary Figure 14. $^{n\mathrm{Pr}}$DMQA$^{\mathrm{NMe2+}}$. Capacity monitoring. Each data point represents one cycle.

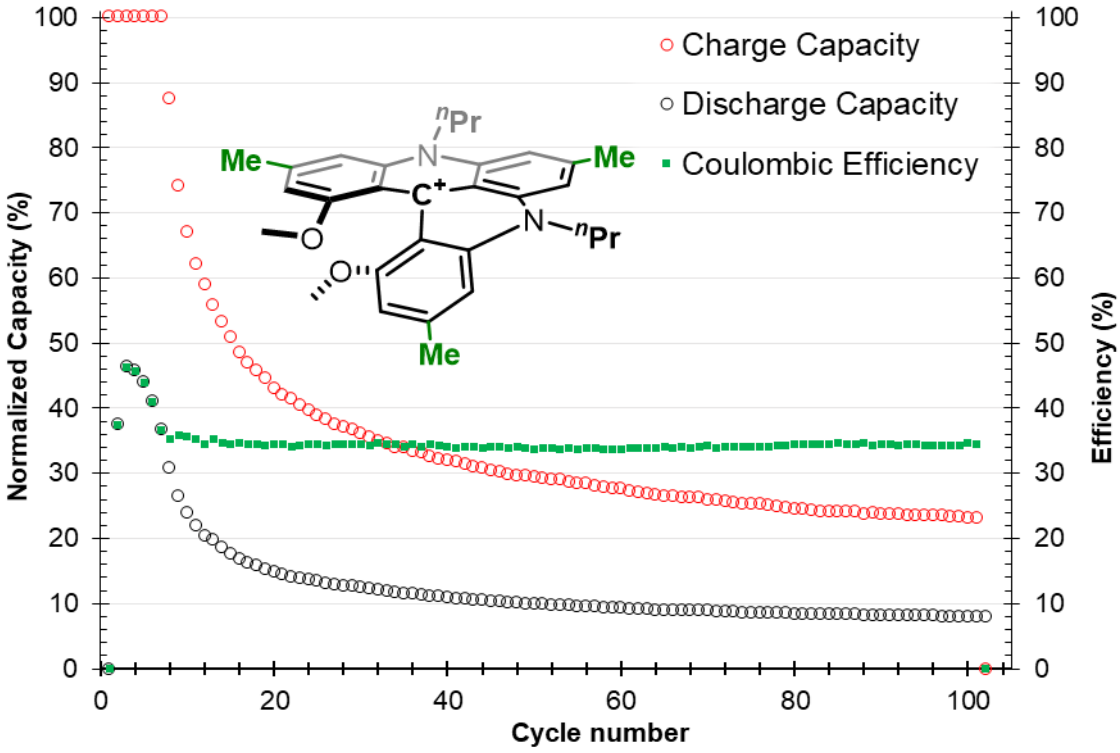

Supplementary Figure 15. $^{n\mathrm{Pr}}$DMQA$^{(p\mathrm{Me})3+}$. Coulombic Efficiency and Capacity monitoring. Each data point represents one cycle.

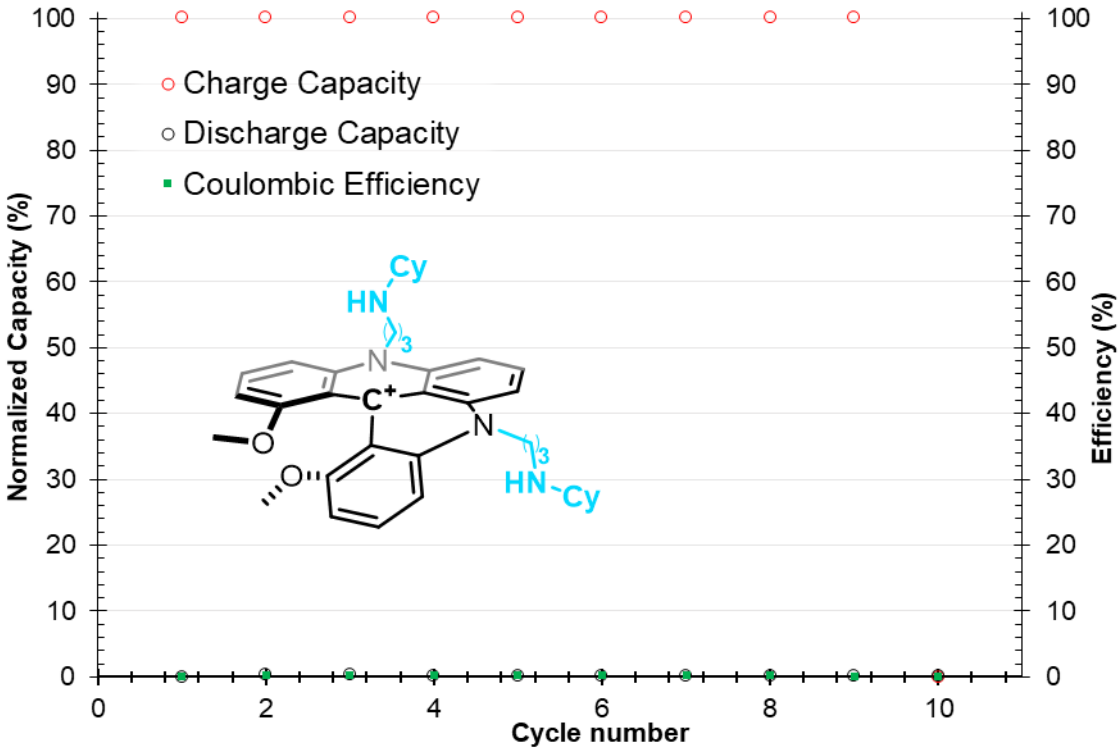

Supplementary Figure 16. $^{(\mathrm{CyNH}n\mathrm{Pr})}$DMQA^{+}. Coulombic Efficiency and Capacity monitoring. Each data point represents one cycle.

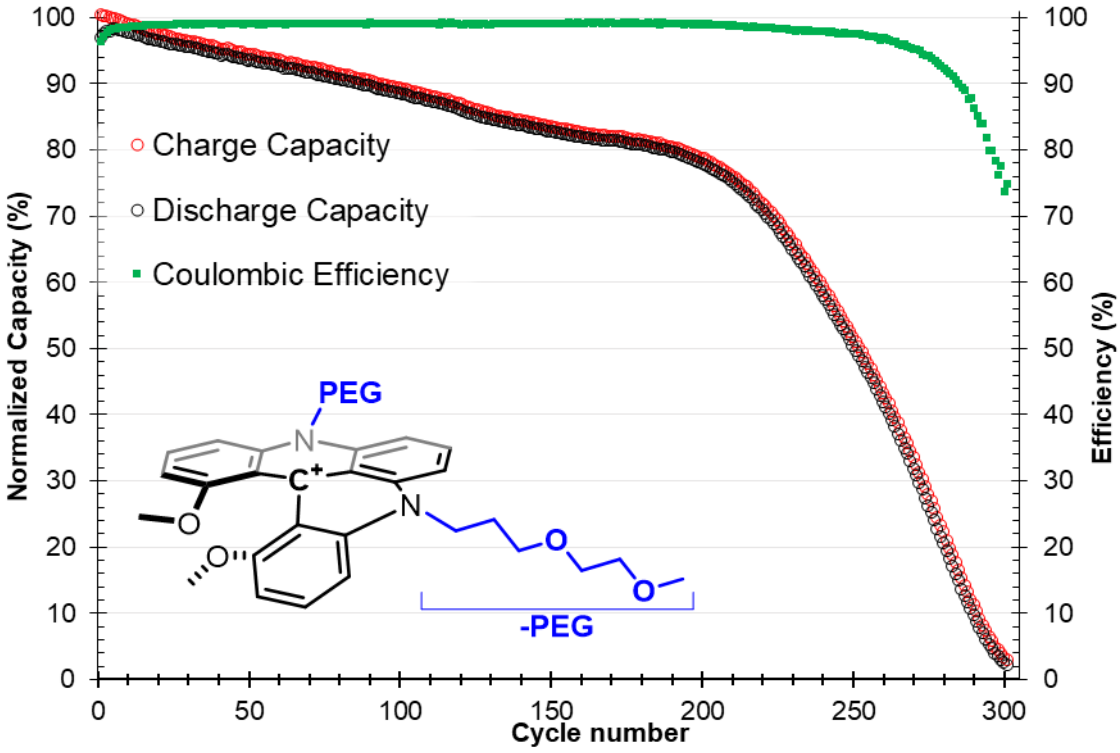

Supplementary Figure 17. $^{PEG}DMQA^{+}$. Coulombic Efficiency and Capacity monitoring. Each data point represents one cycle.

VI. References

1. Mei L., Veleta J. M., Gianetti T. L. Helical Carbenium Ion: A Versatile Organic Photoredox Catalyst for Red-Light-Mediated Reactions. *J. Am. Chem. Soc.* **2020**, *142* (28), 12056–12061, DOI: 10.1021/jacs.0c05507.
2. Moutet J., Veleta J. M., Gianetti T. L. Symmetric, Robust, and High-Voltage Organic Redox Flow Battery Model Based on a Helical Carbenium Ion Electrolyte. *ACS Appl. Energy Mater.* **2021**, *4* (1), 9–14, DOI: 10.1021/acsaem.0c02350.
3. Delgado I. H., Pascal S., Wallabregue A., Duwald R., Besnard C., Guénée L., Nançoz C., Vauthey E., Tovar R. C., Lunkley J. L., Muller G., Lacour J. Functionalized Cationic [4]Helicenes with Unique Tuning of Absorption, Fluorescence and Chiroptical Properties up to the Far-Red Range. *Chem. Sci.* **2016**, *7* (7), 4685–4693, DOI: 10.1039/C6SC00614K.
4. Moutet J., Mills D., Hossain M. M., Gianetti T. L. Increased Performance of an All-Organic Redox Flow Battery Model via Nitration of the [4]Helicenium DMQA Ion Electrolyte. *Mater. Adv.* **2022**, *3* (1), 216–223, DOI: 10.1039/D1MA00914A.
5. Mobian P., Nicolas C., Francotte E., Bürgi T., Lacour J. Synthesis, Resolution, and VCD Analysis of an Enantiopure Diazaoxatricornan Derivative. *J. Am. Chem. Soc.* **2008**, *130* (20), 6507–6514, DOI: 10.1021/ja800262j.
6. Moutet J., Mills D. D., Lozier D. L., Gianetti T. L. [4] Helicenium Ion as Bipolar Redox Material for Symmetrical Fully Organic Pole-Less Redox Flow Battery . *https://chemrxiv.org/engage/chemrxiv/article-details/612d606a90051e2538e50b8e* **2023**, 1–33.
7. Torricelli F., Bosson J., Besnard C., Chekini M., Bürgi T., Lacour J. Modular Synthesis, Orthogonal Post-Functionalization, Absorption, and Chiroptical Properties of Cationic [6]Helicenes. *Angew. Chemie Int. Ed.* **2013**, *52* (6), 1796–1800, DOI: 10.1002/anie.201208926.
8. Laursen B. W., Krebs F. C. Synthesis of a Triazatriangulenium Salt. *Angew. Chemie* **2000**, *39* (19), 3432–3434, DOI: 10.1002/1521-

3773(20001002)39:19<3432::AID-ANIE3432>3.0.CO;2-S.

9. Nicholson R. S. Theory and Application of Cyclic Voltammetry for Measurement of Electrode Reaction Kinetics. *Anal. Chem.* **1965**, *37* (11), 1351–1355, DOI: 10.1021/ac60230a016.

10. Lavagnini I., Antiochia R., Magno F. An Extended Method for the Practical Evaluation of the Standard Rate Constant from Cyclic Voltammetric Data. *Electroanalysis* **2004**, *16* (6), 505–506, DOI: 10.1002/elan.200302851.

11. Yan Y., Robinson S. G., Sigman M. S., Sanford M. S. Mechanism-Based Design of a High-Potential Catholyte Enables a 3.2 V All-Organic Nonaqueous Redox Flow Battery. *J. Am. Chem. Soc.* **2019**, *141* (38), 15301–15306, DOI: 10.1021/jacs.9b07345.

12. Antoni P. W., Bruckhoff T., Hansmann M. M. Organic Redox Systems Based on Pyridinium–Carbene Hybrids. *J. Am. Chem. Soc.* **2019**, *141* (24), 9701–9711, DOI: 10.1021/jacs.9b04249.

VII. Copies of NMR Spectra

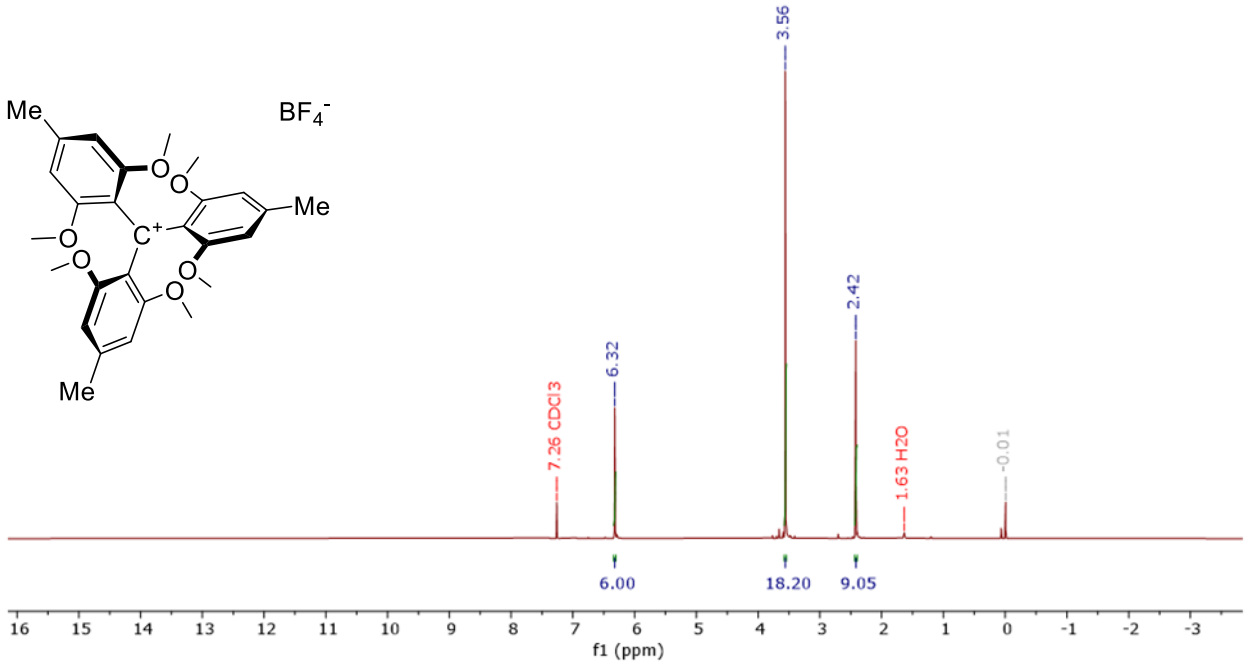

Supplementary Figure 18. ^{1}H spectra (500 MHz, $CDCl_3$) of tris(2,6-dimethoxy-4-methylphenyl)carbenium tetrafluoroborate.

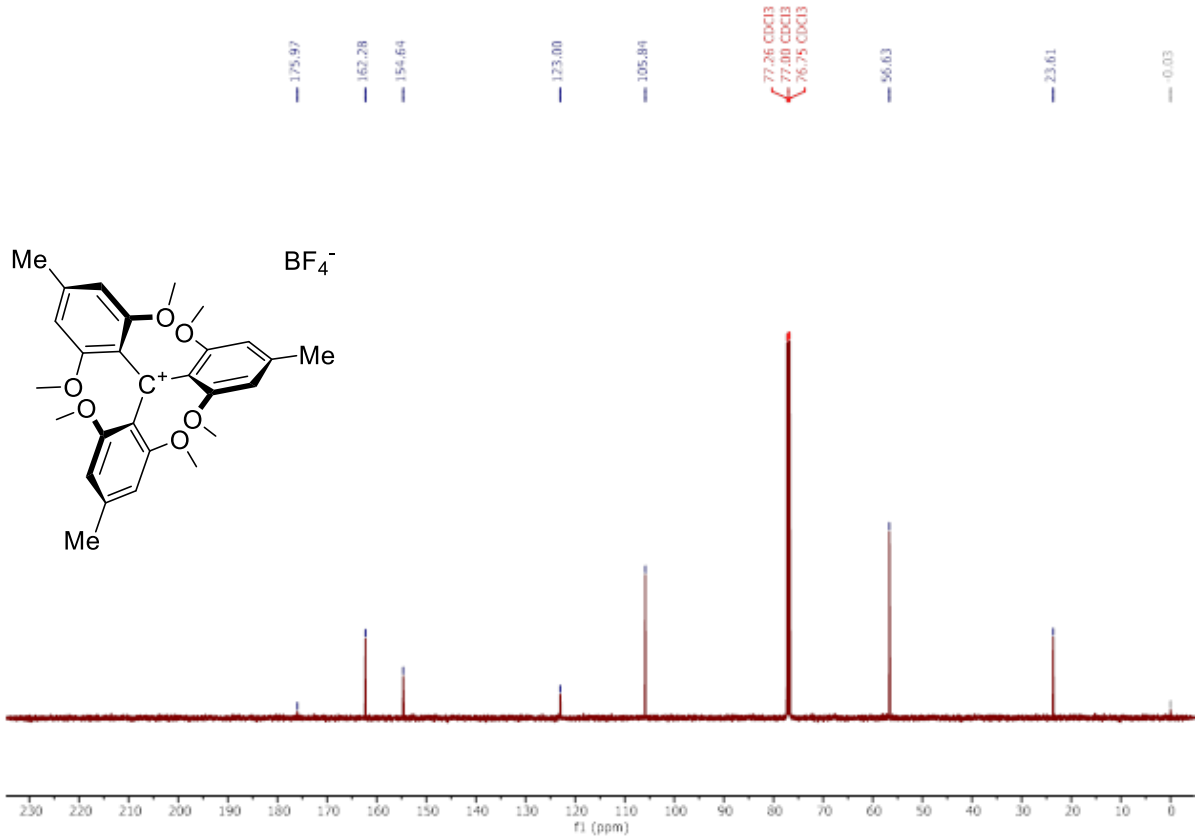

Supplementary Figure 19. ^{13}C{^{1}H} spectra (126 MHz, $CDCl_3$) of tris(2,6-dimethoxy-4-methylphenyl)carbenium tetrafluoroborate.

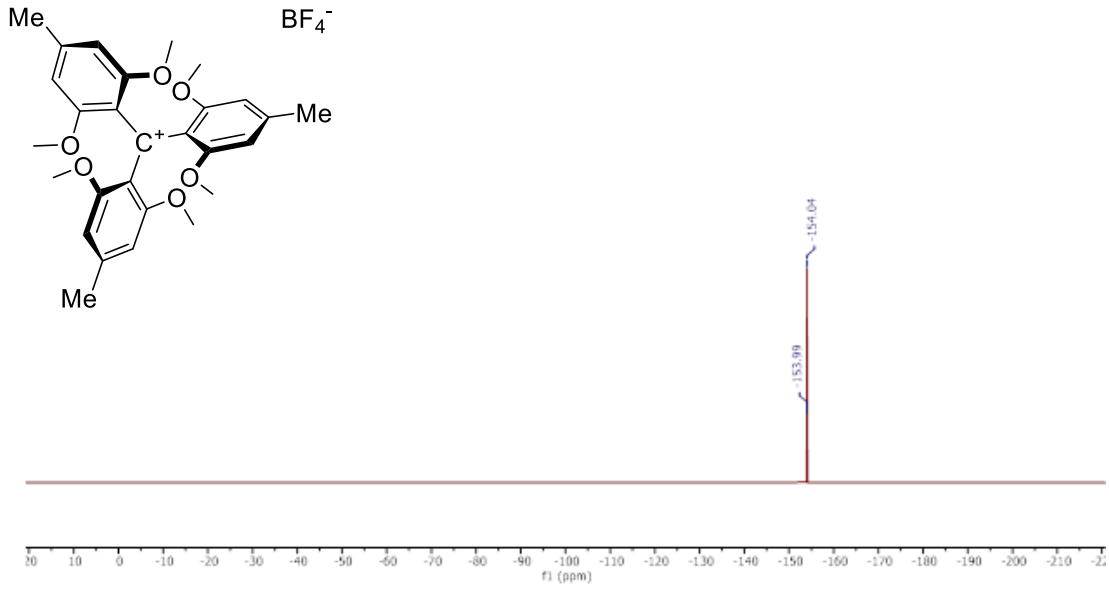

Supplementary Figure 20. $^{19}F\{^{1}H\}$ spectra (471 MHz, $CDCl_3$) of tris(2,6-dimethoxy-4-methylphenyl)carbenium tetrafluoroborate.

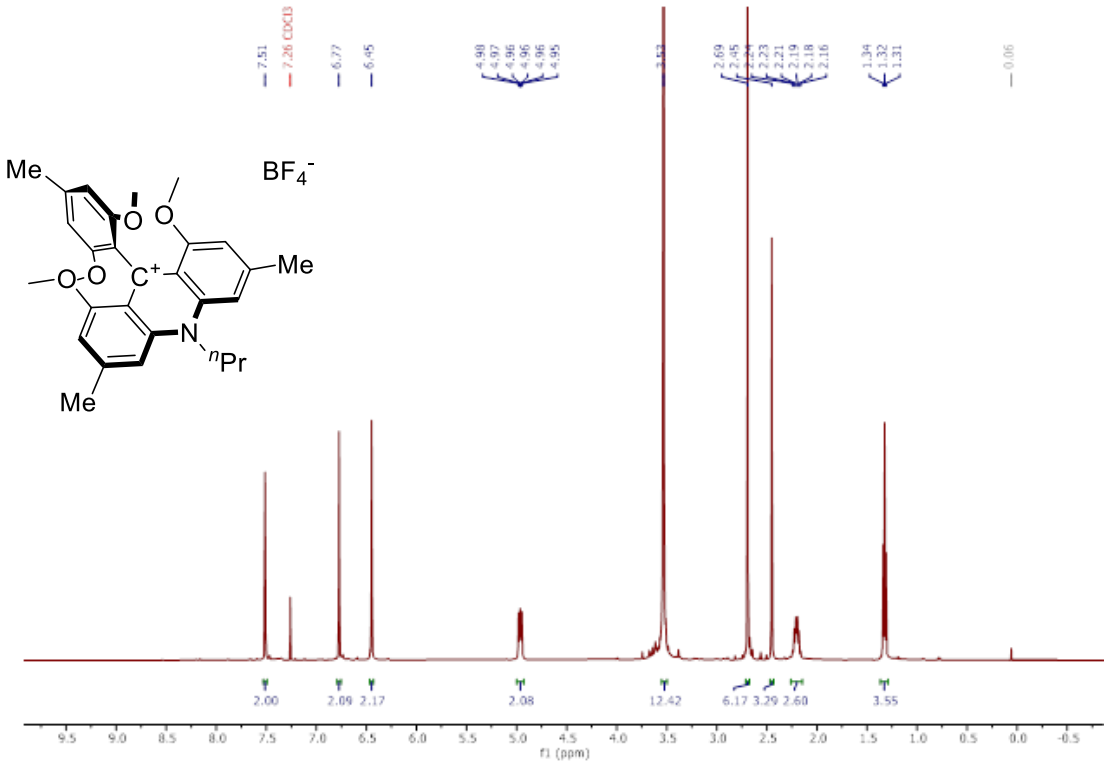

Supplementary Figure 21. ^{1}H spectra (500 MHz, $CDCl_3$) of 9-(2,6-dimethoxy-4-methylphenyl)-1,8-dimethoxy-3,6-dimethyl-10-propyl-9,10-dihydroacridin-9-ylium tetrafluoroborate.

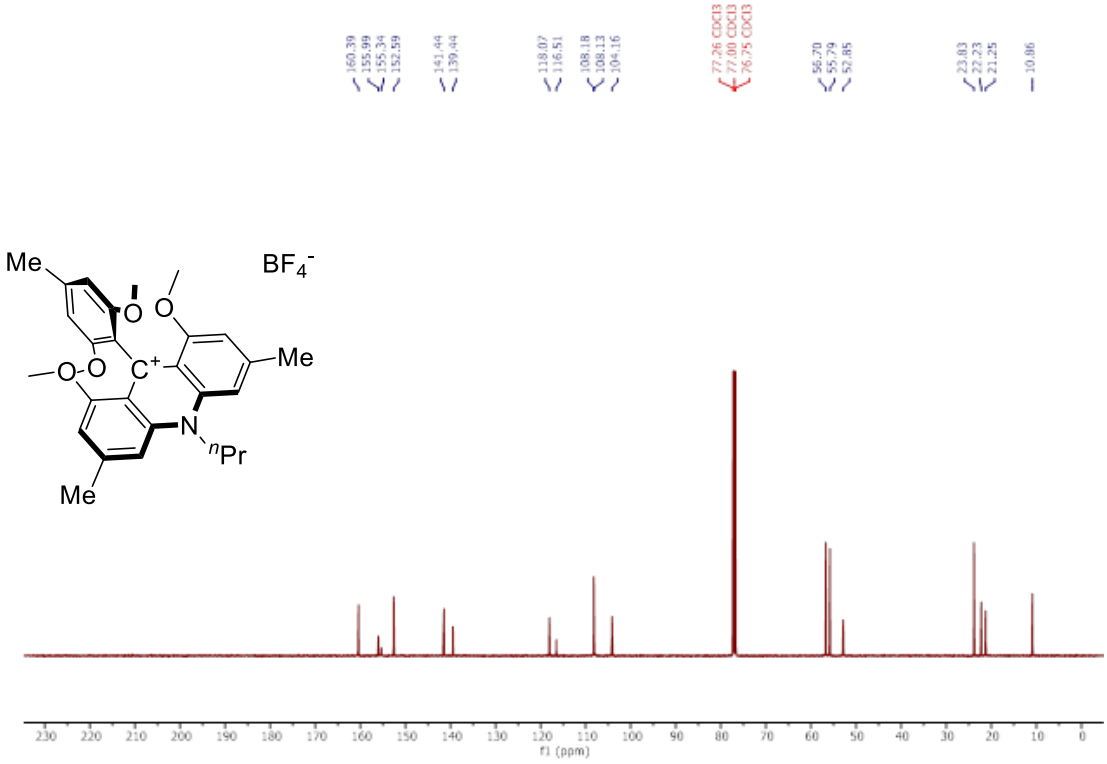

Supplementary Figure 22. ^{13}C{^{1}H} spectra (126 MHz, $CDCl_3$) of 9-(2,6-dimethoxy-4-methylphenyl)-1,8-dimethoxy-3,6-dimethyl-10-propyl-9,10-dihydroacridin-9-ylium tetrafluoroborate.

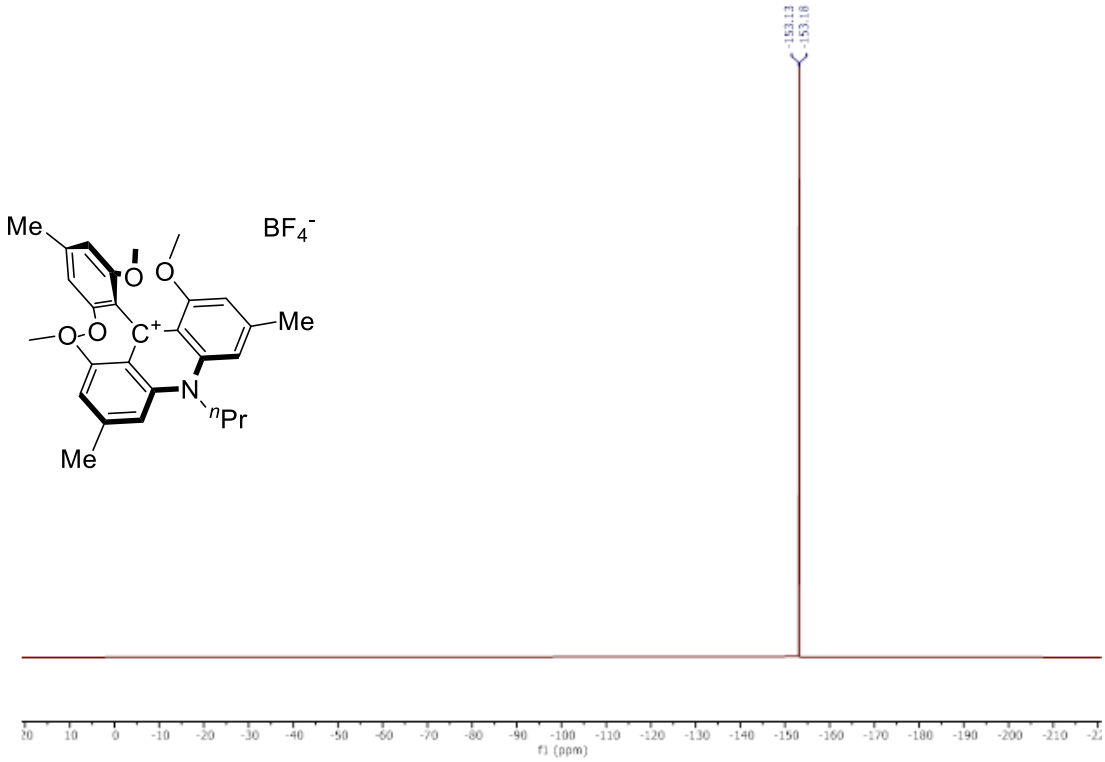

Supplementary Figure 23. $^{19}F\{^{1}H\}$ spectra (471 MHz, $CDCl_3$) of 9-(2,6-dimethoxy-4-methylphenyl)-1,8-dimethoxy-3,6-dimethyl-10-propyl-9,10-dihydroacridin-9-ylium tetrafluoroborate.

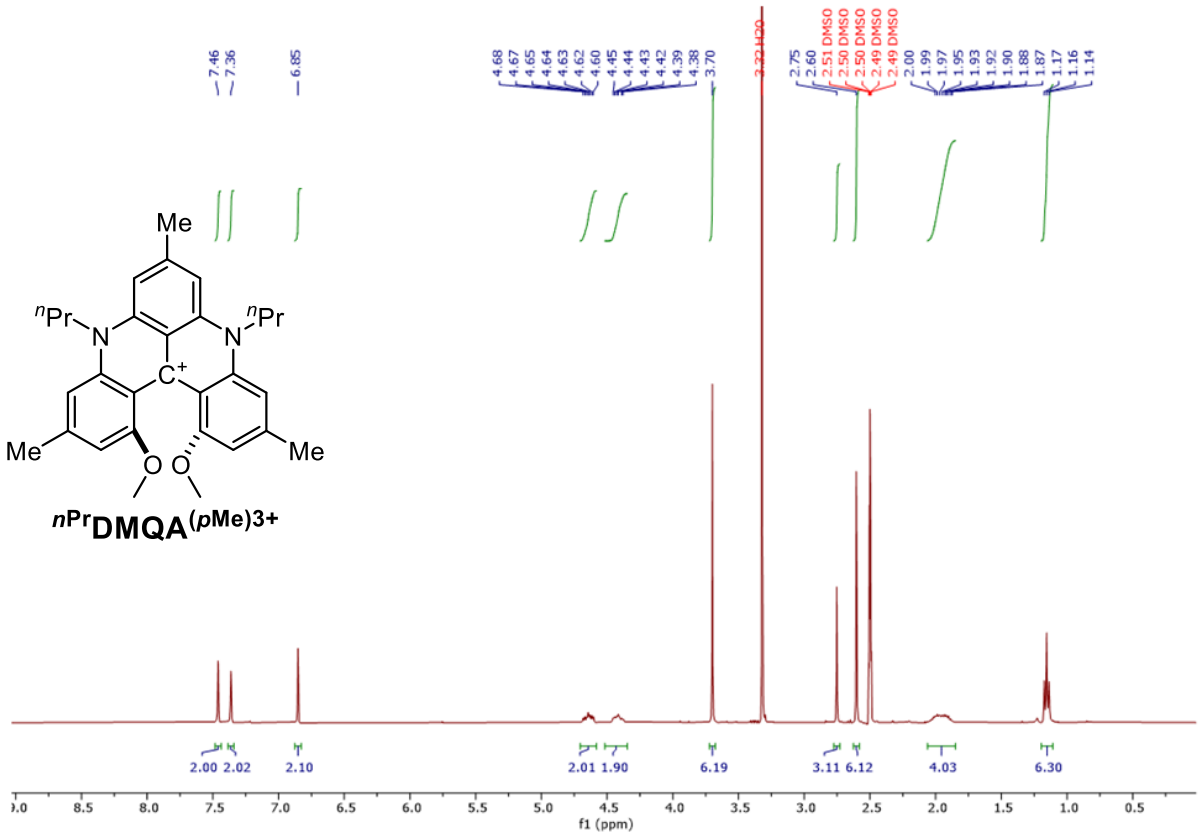

Supplementary Figure 24. ^{1}H spectra (400 MHz, DMSO-d_6) of $^{n\mathrm{Pr}}$DMQA$^{(p\mathrm{Me})3+}$.

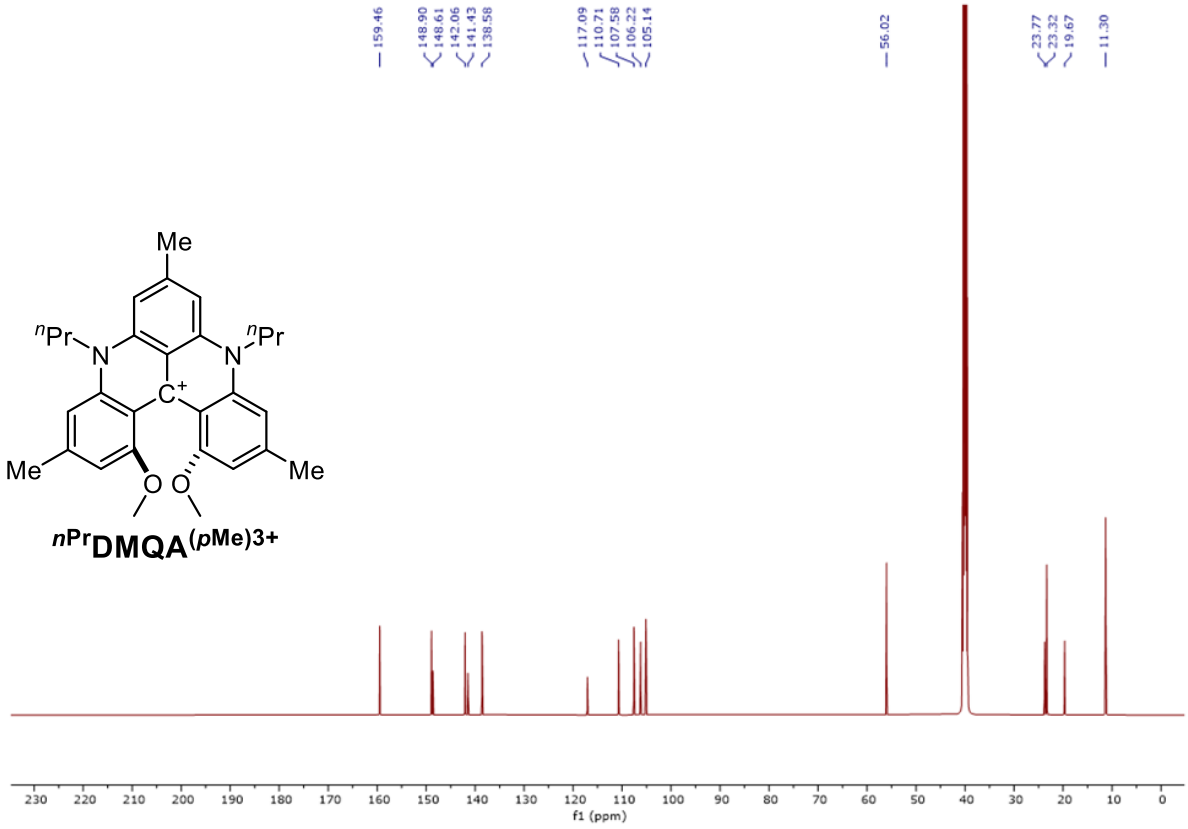

Supplementary Figure 25. ^{13}C{^{1}H} spectra (126 MHz, DMSO-d_6) of $^{n\mathrm{Pr}}$DMQA$^{(p\mathrm{Me})3+}$.

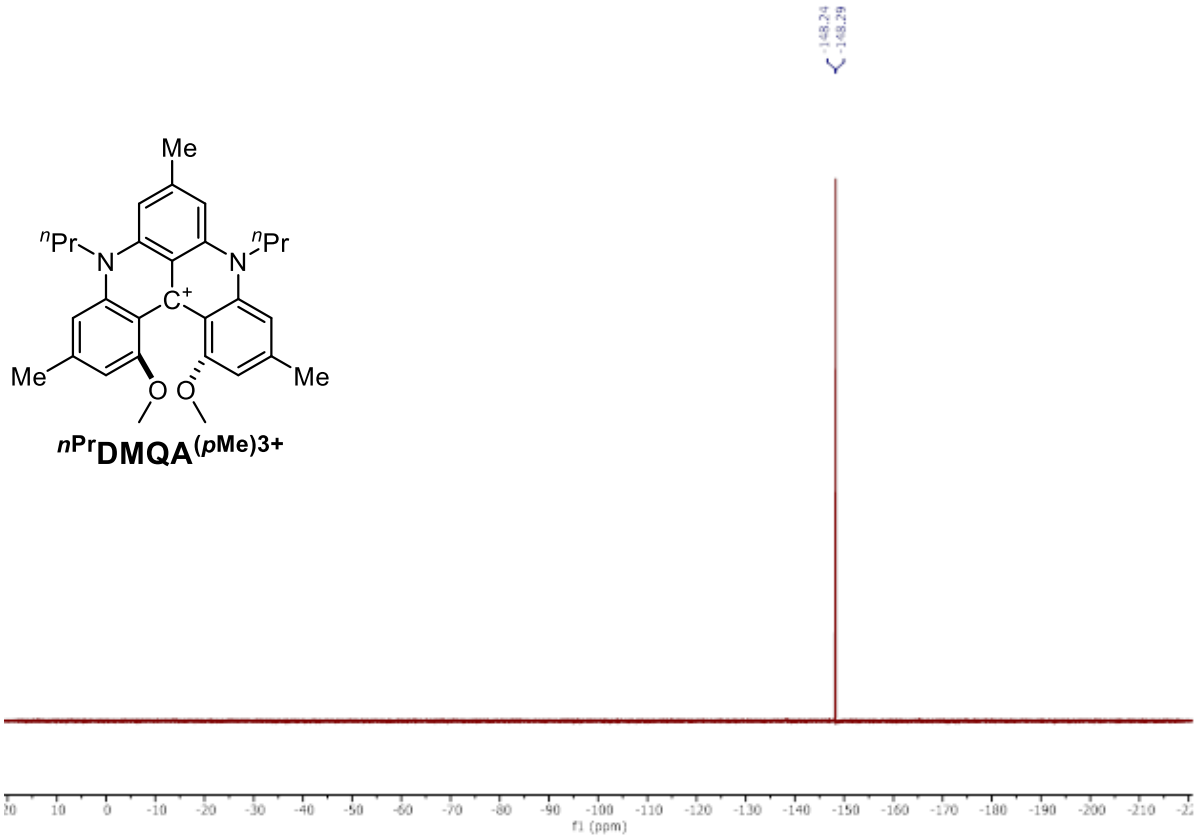

Supplementary Figure 26. $^{19}F\{^{1}H\}$ spectra (471 MHz, DMSO-d_6) of ^{n}PrDMQA$^{(p\mathrm{Me})3+}$.

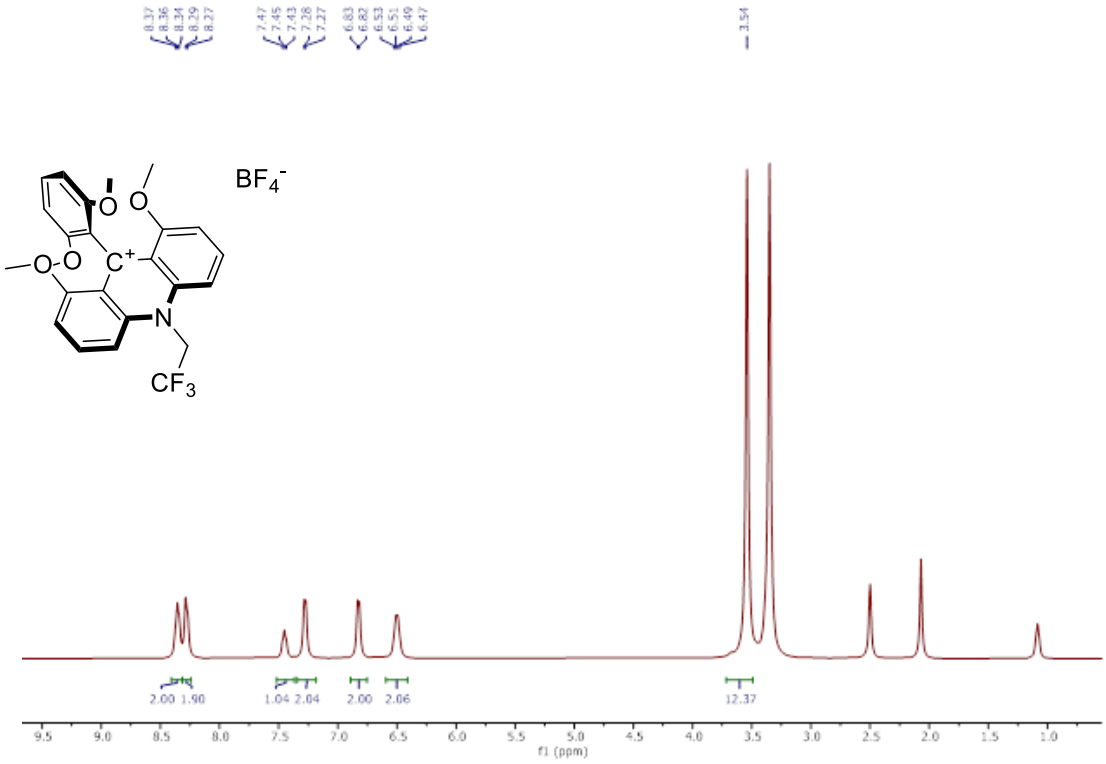

Supplementary Figure 27. ^{1}H spectra (500 MHz, DMSO-d_6) of 9-(2,6-dimethoxyphenyl)-1,8-dimethoxy-10-(2,2,2-trifluoroethyl)-9,10-dihydroacridin-9-ylium tetrafluoroborate

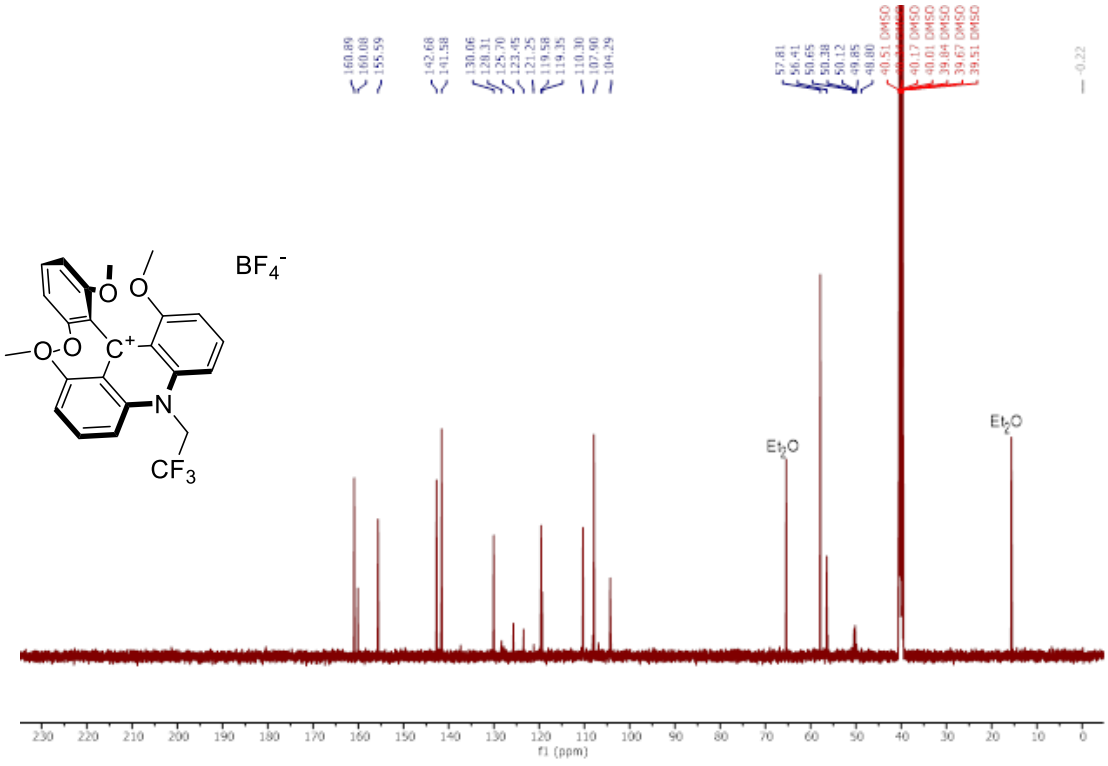

Supplementary Figure 28. ^{13}C{^{1}H} spectra (126 MHz, DMSO-d_6) of 9-(2,6-dimethoxyphenyl)-1,8-dimethoxy-10-(2,2,2-trifluoroethyl)-9,10-dihydroacridin-9-

ylium tetrafluoroborate

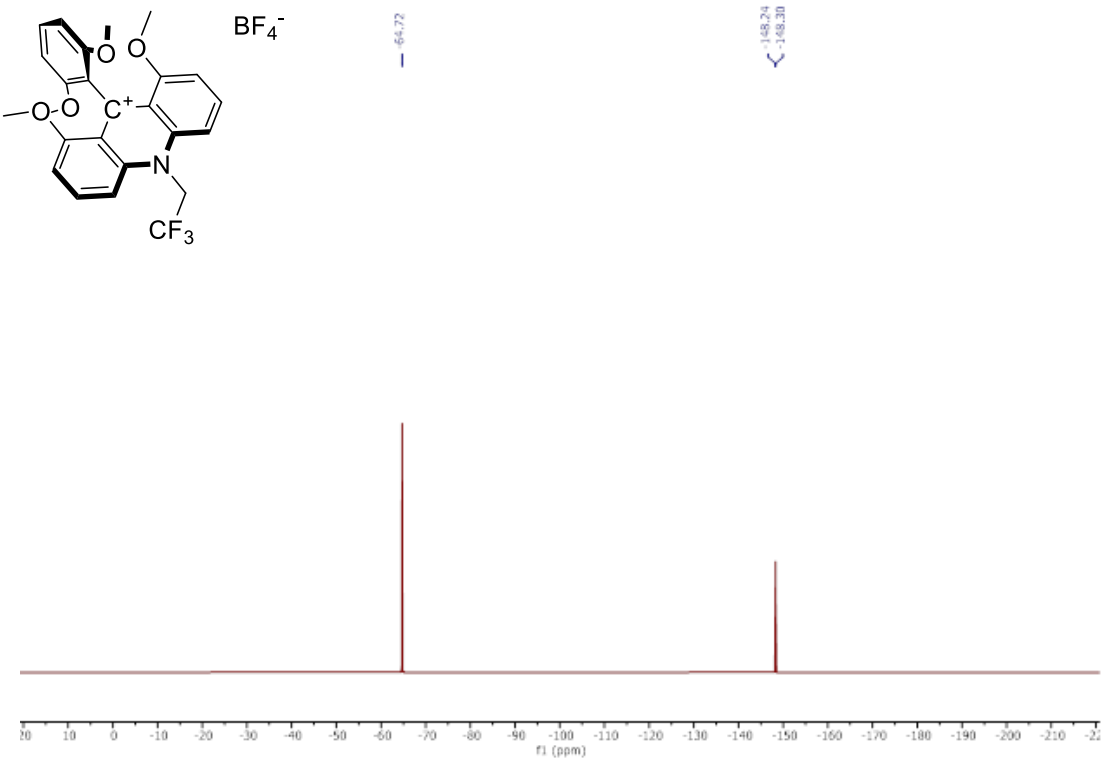

Supplementary Figure 29. $^{19}F\{^{1}H\}$ spectra (471 MHz, DMSO-d_6) of 9-(2,6-dimethoxyphenyl)-1,8-dimethoxy-10-(2,2,2-trifluoroethyl)-9,10-dihydroacridin-9-ylium tetrafluoroborate.

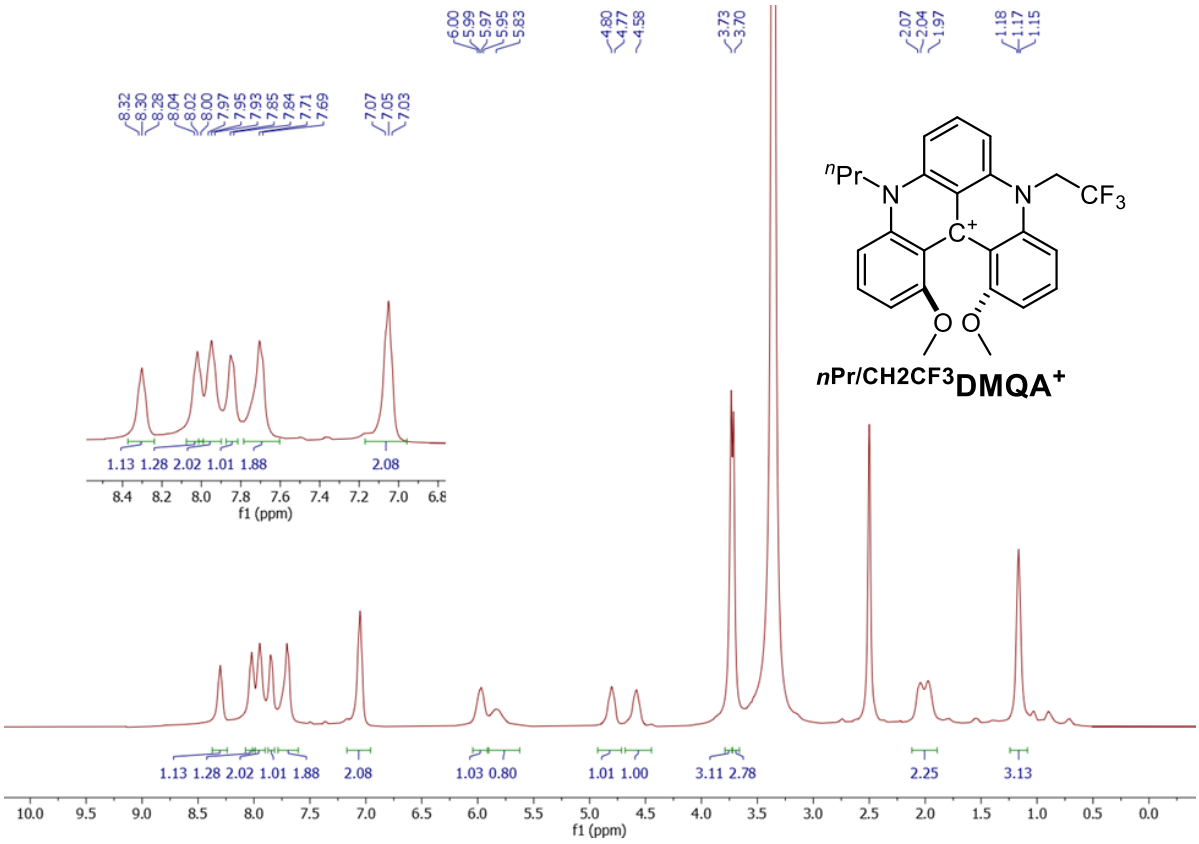

Supplementary Figure 30. ^{1}H spectra (500 MHz, DMSO-d_6) of $^{n\mathrm{Pr/CH2CF3}}$DMQA^{+}.

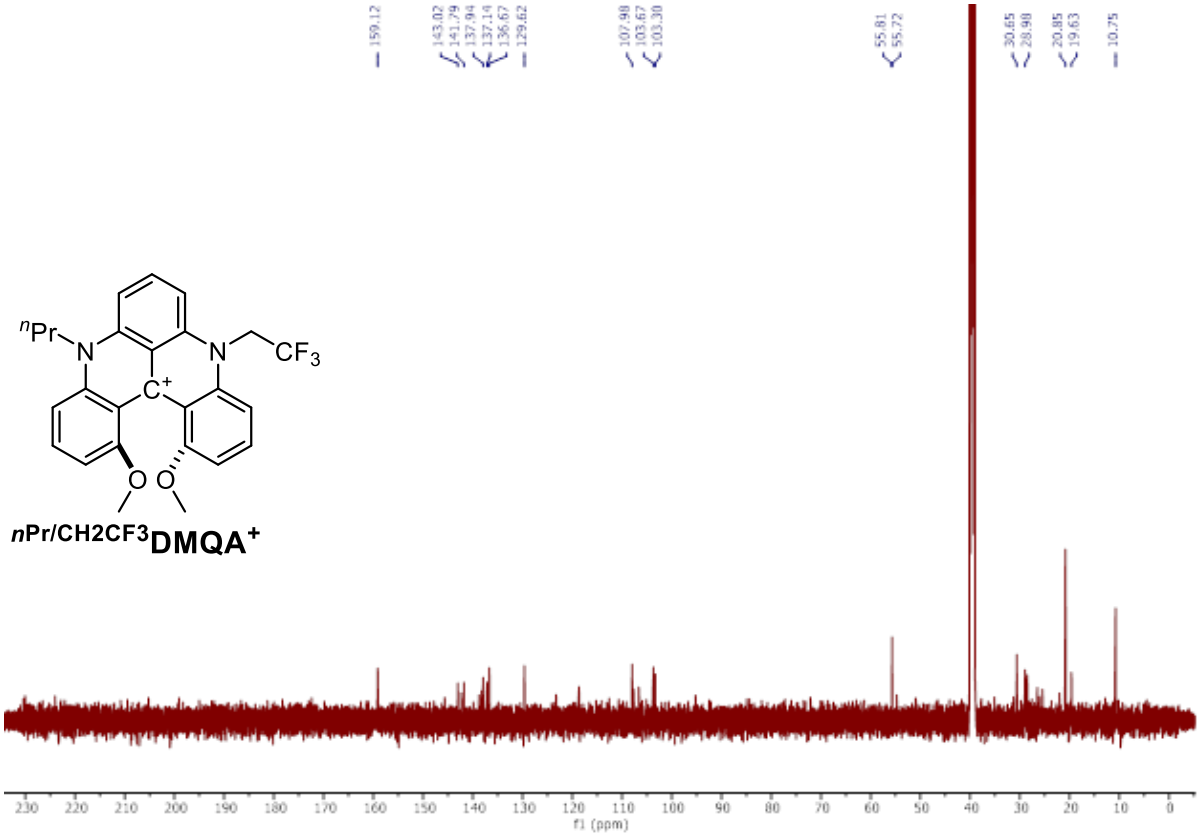

Supplementary Figure 31. ^{13}C{^{1}H} spectra (126 MHz, DMSO-d_6) of $^{n\mathrm{Pr/CH2CF3}}$DMQA^{+}.

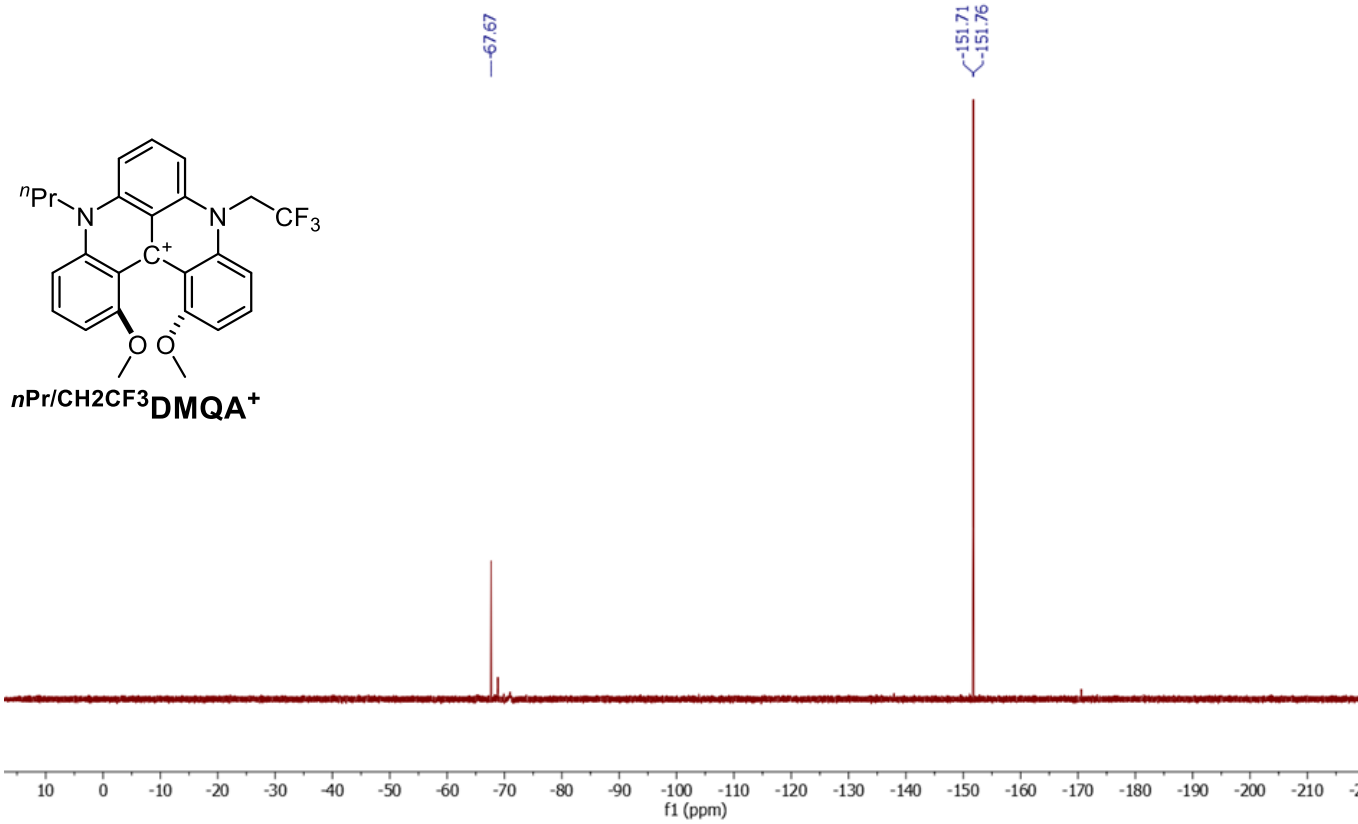

Supplementary Figure 32. $^{19}F\{^{1}H\}$ spectra (471 MHz, DMSO-d_6) of $^{n\mathrm{Pr/CH2CF3}}DMQA^{+}$.

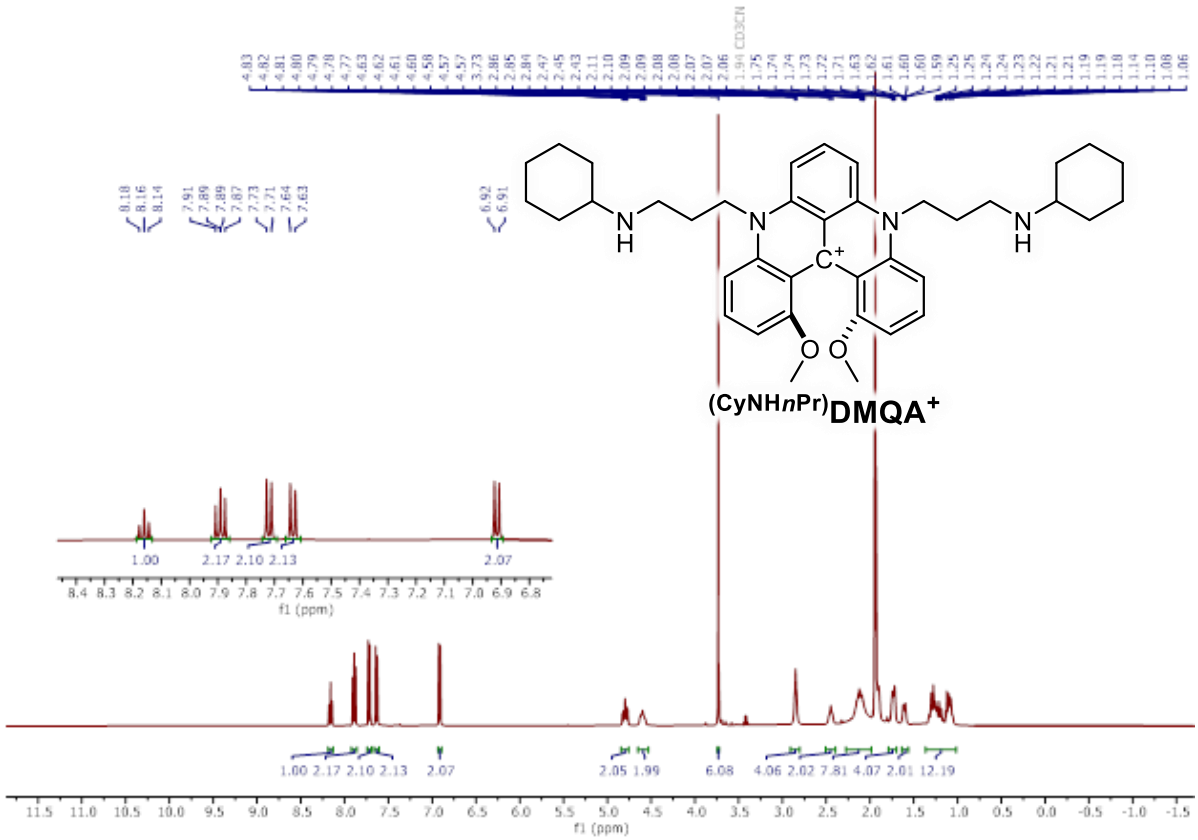

Supplementary Figure 33. ^{1}H spectra (500 MHz, CD_3CN) of $^{(CyNHnPr)}DMQA^{+}$.

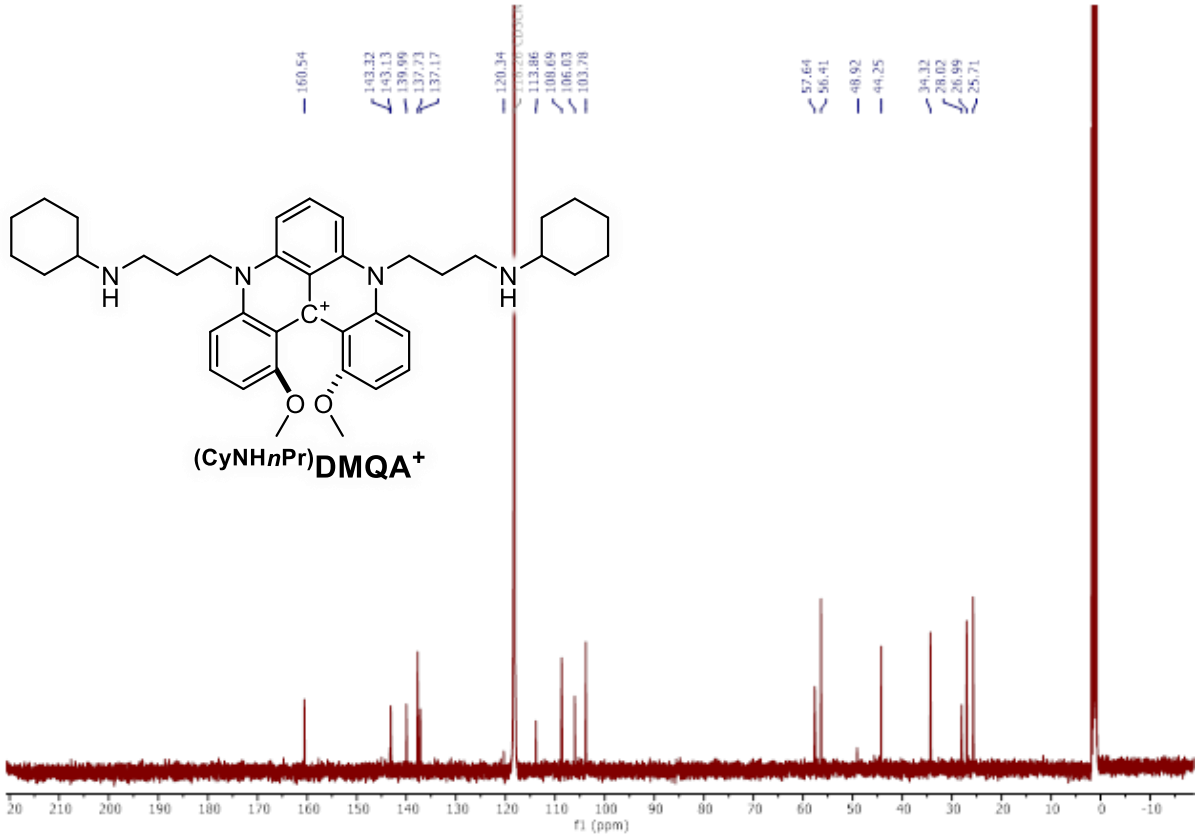

Supplementary Figure 34. $^{13}C\{^{1}H\}$ spectra (126 MHz, CD_3CN) of $^{(CyNHnPr)}DMQA^{+}$.

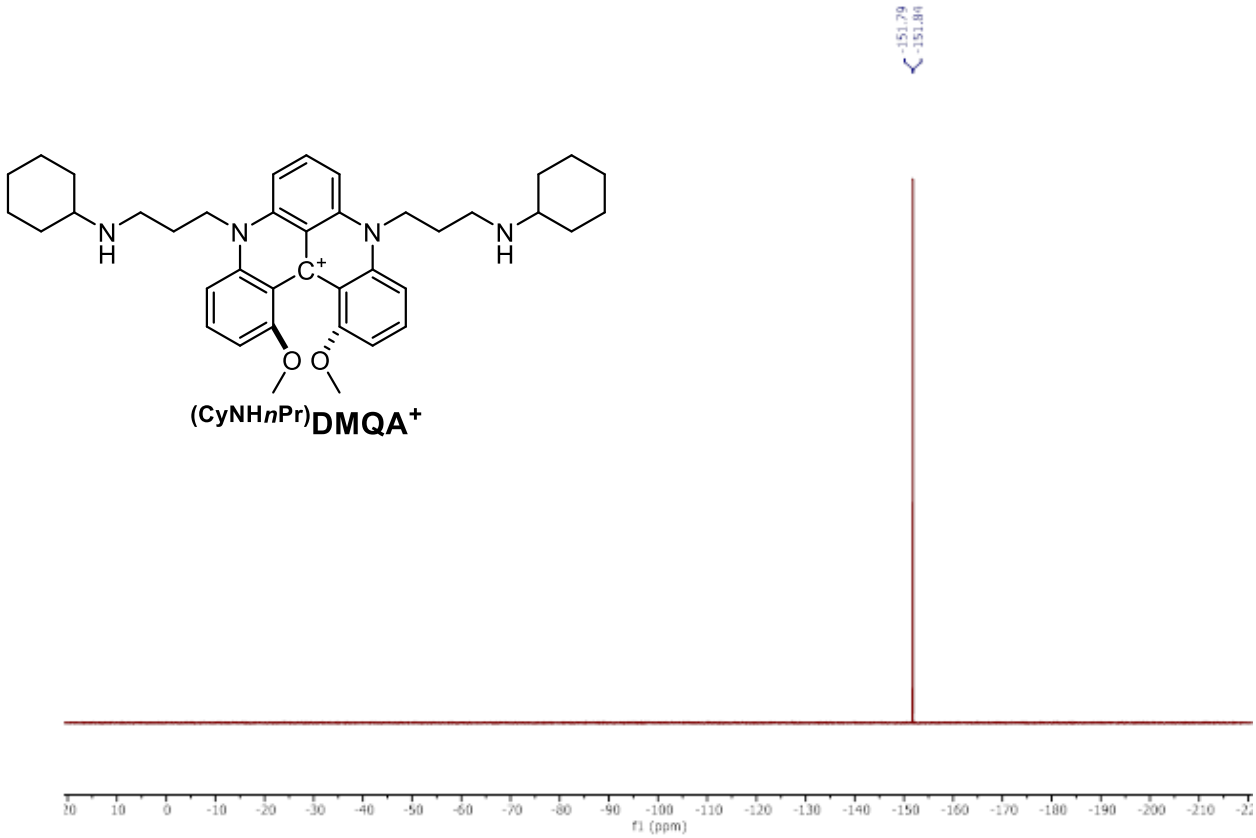

Supplementary Figure 35. $^{19}F\{^{1}H\}$ spectra (471 MHz, CD_3CN) of $^{(CyNH\mathit{n}Pr)}DMQA^{+}$.